A proto-monsoonal climate in the late Eocene of Southeast Asia: Evidence from a sedimentary record in central Myanmar

Huasheng Huang, Robert J Morley, Alexis Licht, Guillaume Dupont-Nivet, Daniel Pérez-Pinedo, Jan Westerweel, Zaw Win, Day Wa Aung, Eko Budi Lelono, Galina N Aleksandrova, et al.

Journal Pre-proofs

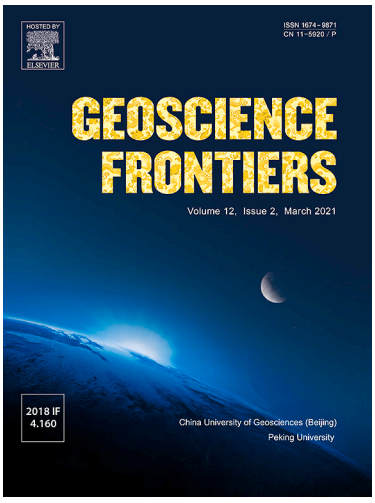

Research Paper

A proto-monsoonal climate in the late Eocene of Southeast Asia: Evidence from a sedimentary record in central Myanmar

Huasheng Huang, Robert J. Morley, Alexis Licht, Guillaume Dupont-Nivet, Daniel Pérez-Pinedo, Jan Westerweel, Zaw Win, Day Wa Aung, Eko Budi Lelono, Galina N. Aleksandrova, Ramesh K. Saxena, Carina Hoorn

PII: S1674-9871(22)00110-4
DOI: https://doi.org/10.1016/j.gsf.2022.101457
Reference: GSF 101457

To appear in: *Geoscience Frontiers*

Received Date: 1 March 2022
Revised Date: 24 July 2022
Accepted Date: 19 August 2022

Please cite this article as: H. Huang, R.J. Morley, A. Licht, G. Dupont-Nivet, D. Pérez-Pinedo, J. Westerweel, Z. Win, D. Wa Aung, E. Budi Lelono, G.N. Aleksandrova, R.K. Saxena, C. Hoorn, A proto-monsoonal climate in the late Eocene of Southeast Asia: Evidence from a sedimentary record in central Myanmar, *Geoscience Frontiers* (2022), doi: https://doi.org/10.1016/j.gsf.2022.101457

Research Paper

A proto-monsoonal climate in the late Eocene of Southeast Asia: Evidence from a sedimentary record in central Myanmar

Huasheng Huang[a,*,†], Robert J. Morley[b,c], Alexis Licht[d], Guillaume Dupont-Nivet[e,f], Daniel Pérez-Pinedo[a,‡], Jan Westerweel[f], Zaw Win[g], Day Wa Aung[h], Eko Budi Lelono[i], Galina N. Aleksandrova[j], Ramesh K. Saxena[k], Carina Hoorn[a]

[a]Institute for Biodiversity and Ecosystem Dynamics (IBED), University of Amsterdam, 1090 GE Amsterdam, The Netherlands
[b]Palynova Ltd., 1 Mow Fen Road, Littleport, Cambridgeshire CB6 1PY, UK
[c]Department of Earth Sciences, Royal Holloway, University of London, Egham, Surrey TW20 0EX, UK
[d]Centre de Recherche et d'Enseignement de Géosciences de l'Environnement (CEREGE), Aix-en-Provence, France
[e]Institut für Geowissenschaften, Universität Potsdam, 14476 Potsdam, Germany
[f]Géosciences Rennes, CNRS and Université de Rennes 1, 35042 Rennes Cedex, France
[g]Geology Department, Shwe Bo University, Sagaing Region, Myanmar
[h]Department of Geology, University of Yangon, Pyay Road, Yangon, Myanmar
[i]Badan Geologi, Jl. Soekarno Hatta No 444, Bandung, Bandung 40254, Indonesia
[j]Geological Institute, Russian Academy of Sciences, Pyzhevsky Pereulok 7, 119017 Moscow, Russia
[k]Birbal Sahni Institute of Palaeosciences, 53 University Road, Lucknow-226 007, India

*Corresponding author.
E-mail address: buxushuang@gmail.com, huasheng.huang@unifi.it (H. Huang).
[†]Present address: Department of Earth Sciences, University of Florence, Via G. La Pira 4, 50121 Florence, Italy.
[‡]Present address: Department of Earth Sciences, Memorial University of Newfoundland, St. John's, Newfoundland A1B 3X5, Canada.

Handling Editor: V.O. Samuel

Abstract

The Burma Terrane has yielded some of the earliest pieces of evidence for monsoonal rainfall in the Bay of Bengal. However, Burmese ecosystems and their potential monsoonal imprint remain poorly studied. This study focuses on the late Eocene Yaw Formation (23° N) in central Myanmar, which was located near the equator (*c.* 5° N) during the Eocene. We quantitatively assessed the past vegetation, climate, and depositional environments with sporomorph diagrams, bioclimatic analysis, and sequence biostratigraphy. We calculated the palynological diversity and drew inferences with rarefaction analysis by comparing with four other middle to late Eocene tropical palynofloras. Palynological results highlight a high floristic diversity for the palynoflora throughout the section formed by six pollen zones characterized by different vegetation. They indicate that lowland evergreen forests and swamps dominated in the Eocene Burmese deltaic plains while *terra firma* areas were occupied by seasonal evergreen, seasonally dry, and deciduous forests. This vegetation pattern is typical to what is found around the Bay of Bengal today and supports a monsoon-like climate at the time of the Yaw Formation. Bioclimatic analysis further suggests that in the late Eocene, the Yaw Formation was more seasonal, drier, and cooler compared to modern-day climate at similar near-equatorial latitude. More seasonal and drier conditions can be explained by a well-marked seasonal migration of the Intertropical Convergence Zone (ITCZ), driver of proto-monsoonal rainfall. Cooler temperatures in the late Eocene of central Myanmar may be due to the lack of adequate modern analogues for the Eocene monsoonal climate, while those found at other three Eocene Asian paleobotanical sites (India and South China) may be caused by the effect of canopy evapotranspirational cooling. Our data suggest that paleoenvironmental change including two transgressive-regressive depositional sequences is controlled by global sea level change, which may be driven by climate change and tectonics. The high diversity of the Yaw Formation palynoflora, despite well-marked seasonality, is explained by its cross-roads location for plant dispersals between India and Asia.

Keywords: Bioclimatic analysis; Diversity; Monsoon; Palynology; Sequence biostratigraphy; Southeast Asia.

1. Introduction

The Asian monsoons, a term principally grouping the South Asian Monsoon (SAM) and the East Asian Monsoon (EAM), are today the most intricate monsoon system around the globe (Molnar et al., 2010; Spicer, 2017). The SAM affects India, the Indochina Peninsula, and the South China Sea, while the EAM influences the precipitation patterns over China, the Korean Peninsula, and Japan (e.g., Wang and Ho, 2002; Molnar et al., 2010). Monsoons are defined by annual surface wind inversion (Ramage, 1971) and by annual reversals in heating and temperature gradients between continents and oceans with the progression of the seasons (Trenberth et al., 2006). Based on field observational evidence (i.e., non-modelling results), the initiation of the Asian monsoons is thought to be as early as the early Miocene (e.g., Guo et al., 2002; Clift et al., 2008; Morley, 2012) or the late Oligocene (Srivastava et al., 2012). More recently, quantitative reconstructions of past precipitation based on stable isotopes and paleobotanical data have suggested the existence of monsoonal rainfall during the middle to late Eocene of Asia (e.g., Licht et al., 2014; Herman et al., 2017; Su et al., 2020). These Eocene "proto-monsoons" were possibly driven by seasonal migrations of the Intertropical Convergence Zone (ITCZ) (Spicer, 2017), and their existence has been corroborated by modelling results (e.g., Farnsworth et al., 2019). However, the presence of a modern-like monsoonal circulation during the Eocene is debated (Tardif et al., 2020), and the extant and climatic features of Eocene proto-monsoons remain to be drawn.

Paleobotany has been an effective tool when quantifying monsoonal intensity. Climate-Leaf Analysis Multivariate Program (CLAMP, http://clamp.ibcas.ac.cn), using fossil leaf morphological traits, is the most common method, and has been applied to reconstruct monsoonal signals from the Asian Paleogene, such as in the middle Eocene (*c.* 47 Ma) central Tibet (Su et al., 2020), India (Shukla et al., 2014; Bhatia et al., 2021), the middle Eocene–early Oligocene of southern China (Spicer et al., 2016; Herman et al., 2017) and even early to middle Eocene in the Antarctic (Jacques et al., 2011).

In the Minbu Basin (southern part of the Central Myanmar Basins, CMB), a proto-monsoonal climate, likely favored by Eocene greenhouse conditions, was suggested for the late middle Eocene Pondaung Formation, based on low oxygen isotope values with strong seasonality in gastropod shells and mammal teeth (Licht et al., 2014). Coexistence and wood anatomical approaches that were applied on fossil wood specimens from the same formation also corroborates the existence of a proto-monsoonal climate (Licht et al., 2015).

In the Chindwin Basin, northern part of the CMB, a long and well-exposed Cenozoic stratigraphic record in Kalewa was recently dated using multiple proxies (U-Pb zircon dating, Licht et al., 2019; magnetostratigraphy, U–Pb apatite dating, and apatite fission track dating,

Westerweel et al., 2020; and palynostratigraphy, Huang et al., 2020). The paleoenvironments of the late middle to late Eocene Yaw Formation in Kalewa have been well documented from sedimentological (Licht et al., 2019; Westerweel et al., 2020), and palynological studies (Huang et al., 2020, 2021). The palynological composition of the Yaw Formation suggests a representation of evergreen forests with drier vegetation away from the area of sedimentation, and a predominance of palms, Sapotaceae, and mangrove elements (Huang et al., 2021). The paleoenvironments and palynological composition of the Yaw Formation may be driven by a proto-monsoonal climate similar to the Pondaung Formation together with tectonics. Therefore, a quantitative and comprehensive evaluation of the sporomorph composition is needed to spatiotemporally investigate the early history of vegetation and proto-monsoonal climate in the CMB.

Sequence biostratigraphy, which examines sporomorph distribution patterns and correlates this to climate change and tectonics, is based on sporomorph compositional change and has been a successful tool in analyzing the depositional environments in the Cenozoic of SE Asia (e.g., Vietnam, Morley et al., 2019, and Nguyen et al., 2021; Malaysia, Morley et al., 2021). Hence it is significant to investigate the depositional environments in the CMB and correlate these to climate change in a sequence biostratigraphic framework. Furthermore, past floristic diversity patterns, which may be driven by climate and paleogeography (i.e., paleolocation affected by tectonics), can also be attained by palynological analysis applying multiple methods, such as rarefaction analysis, Simpson index, Bootstrap, and range-through method, and thus relate to possible drivers (such as, paleoclimate and paleogeography) (e.g., Jaramillo and Dilcher, 2000; Jaramillo et al., 2006, 2010).

In this study, we present the palynological data from the Yaw Formation with comprehensive sporomorph diagrams to reconstruct vegetation changes throughout the late Eocene in the CMB (Fig. 1a and b). We also evaluate the data in a sequence biostratigraphic framework to unravel the dynamics of the depositional environments throughout the section. Additionally, we use bioclimatic analysis to quantitatively reconstruct the climate based on the main climatic variables. We apply the rarefaction method to analyze the sporomorph diversity in the Yaw Formation and compare this with four other middle to late Eocene tropical sporomorph assemblages. This enables us to estimate how climate change and tectonics stimulated plant diversity. Together, these analyses allow us to understand the relation between vegetation, depositional environments, and plant diversity with climate and geological driving factors in the late Eocene CMB.

2. Regional setting

2.1. Geological context

The Kalewa study area is situated in the CMB and comprises an almost continuous succession of Cenozoic sedimentary rocks that were mostly deposited in fluvio-deltaic environments (Licht et al., 2013, 2019) (Fig. 1a and b). The study area is limited to the east by the Sino-Burman Ranges (SBR) (Fig. 1b), comprising the Yunnan highlands, the Shan Plateau, and the Tenasserim Range (Fig. 2b), all belonging to the local units of the Sibumasu Terrane (Metcalfe, 2013). On the western side, the basin is separated from the Bay of Bengal by the Indo-Burman Ranges (IBR, Fig. 1b; Maurin and Rangin, 2009). During the late middle Eocene, the BT was at a near-equatorial position and situated along the Neotethyan margin (*c.* 5° N for our study site, see Fig. 1c; Westerweel et al., 2019, 2020). The CMB was open to the Indian Ocean and was the locus of SW-directed deltas (Licht et al., 2013, 2019), most probably sourced in eastern and northern Myanmar (Westerweel et al., 2020). Incipient uplift of the IBR at the time of the Yaw Formation resulted in the set-up of islands west of the Burmese coastlines, resulting in semi-enclosed estuarine conditions in the CMB (Licht et al., 2019).

The Cenozoic sedimentary sequence exposed in Kalewa starts with the Pondaung Formation followed by the Yaw Formation (Fig. 1a), both of Eocene age and deposited in fluvio-deltaic environments. The Yaw Formation is mainly formed of sandstones, mudstones, and lignites all rich in fossil leaf fragments. The sediments were deposited in an onshore fluvio-deltaic to deltaic environment exiting in a wide barrier-bound estuarine system (Licht et al., 2019). The uppermost horizon of the Yaw Formation is unconformably overlain by the fluvial sandstones of the Tonhe Formation, formerly considered as part of the Miocene Letkat Formation but recently recognized as an earlier Oligocene unit (Westerweel et al., 2020). The contact presents erosional features characteristic of incised fluvial channels, and its base can be regarded as a sequence boundary (Moe Zat and Day Wa Aung, 2018), and an erosional unconformity.

2.2. Modern-day climate in Myanmar

The India-Asia collision produced the highest mountains on Earth, including the Tibetan Plateau, the Himalayas, and the SBR, which enhance monsoonal rainfall (Prell and Kutzbach, 1992; Xie et al., 2006; Boos and Kuang, 2010; Ding et al., 2017; Bhatia et al., 2021). Myanmar climate is also modulated by the El Niño-Southern Oscillation and the Indian Ocean Dipole (Ashok et al., 2010). The SAM is the predominant moisture conveyor in Myanmar and approximately 90% of the annual precipitation occurs during the summer season, from mid-May to mid-October (Htway and Matsumoto, 2011). The highest rainfall amount is reached along the Arakan and Tenasserim coast (Fig. 2b). The IBR have a strong rain shadow effect on monsoonal precipitation (Fig. 2b) and rainfall amount significantly decreases landward (de Terra, 1944).

In Myanmar there are three climatic regions: (1) the dry belt in central Myanmar with a mean precipitation (MAP) of less than 1,000 mm given their sheltered location leeward of the IBR (Fig. 2b), which is insufficient to allow forest growth; (2) regions presenting 1,000 to 2,000 mm of MAP

hosting most of the monsoon forests; (3) regions presenting over 2,000 mm of MAP hosting evergreen tropical forests (Stamp, 1925). Based on Köppen-Geiger climate classification maps (Beck et al., 2018), Myanmar is characterized by tropical monsoon, tropical wet and dry or savanna, hot semi-arid, and monsoon-influenced humid subtropical climate types (Fig. 2c). The Kalewa area is situated in the foothills of the IBR and a transitional area between the dry belt and moist deciduous forests (Fig. 2). It falls into the regions presenting 1,000–2,000 mm (region 2) of rainfall hosting a tropical wet and dry or monsoon-influenced humid subtropical climate and most of the monsoon forests stated in Stamp (1925). The adjacent southeastern dry belt in central Myanmar possesses a MAP of ~500–800 mm (Stamp, 1925; Lai Lai Aung et al., 2017). Based on the climate data of five nearby climate stations (Kalewa, Kalamyo, Minkin, Mawlaik, and Varr), the Kalewa study area has MAP values ranging from *c.* 900–1700 mm, with the Kalewa climate station indicating 1641 mm (Lai Lai Aung et al., 2017).

3. Materials and methods

3.1. The studied section

The Kalewa section is a 627.5 m-thick sedimentary sequence that is exposed at the western side of the Kalewa Township, Sagaing Region, NW Myanmar (23°14′ N, 94°15′ E) (Figs. 1 and 2). In this study we included two additional samples situated below this section (23°15′ N, 94°15′ E). The Kalewa section is located at the southern edge of the Chindwin Basin, which belongs to the CMB (Licht et al., 2019; Fig. 1). U–Pb dating of a tuff layer (Licht et al., 2019), magnetostratigraphy, U–Pb apatite dating and apatite fission track dating (Westerweel et al., 2020) provide an age of *c.* 38–37 Ma (Fig. 3), which is also supported by the palynological evidence discussed below and in Huang et al. (2018, 2020). The lowest two samples show an age of *c.* 40–38 Ma (Licht et al., 2019).

3.2. Samples and palynological processing

In 2016 and 2017, 83 rock samples were collected in Kalewa area from fine-grained sandstones and mudstones of the Yaw Formation. Of these, 81 samples belong to the 627.5 m-thick Kalewa section, while two samples are respectively at ~250 m and ~500 m below the base of this section, representing the base of Yaw Formation (Fig. 3).

Two palynological processing methods were performed to ensure maximum recovery. One set of samples was processed for quantitative analysis. The processing was as follows: 1.3 grams of sample was boiled in 10% sodium pyrophosphate, and then treated with 10% HCl, and sieved with 5 µm and 212 µm meshes. The sample was then heated in acetolysis mixture to 100 °C. Bromoform-treatment was applied to separate any remaining inorganic fraction to produce residue. A second set of selected samples was processed mainly for microphotography. The

processing method was as follows: 30 grams of washed and dried sample was treated with 10% HCl and 40% HF. Then a heavy liquid separation was used to separate the organic and remaining inorganic fractions. All resulting residues were mounted on a slide in glycerin and sealed with paraffin for light microscope (LM) observation. Residues were further used for analysis with LM and scanning electron microscopy (SEM) at the Department of Palaeontology (DoP), University of Vienna, Austria. Details on the two methods were presented in Huang et al. (2020).

3.3. Palynological analysis and microphotography

In total, 56 samples were productive for pollen analysis and with a pollen count of *c.* 100 specimens or more. The identification of specimens was carried out using the palynological literature from the America, China, Thailand, India, and Vietnam, and particularly from regions in the proximity of the Kalewa section, such as Assam (India) and Tibet (China) (e.g., Germeraad et al., 1968; Sah and Dutta, 1966; Morley, 1998, 2013; Jaramillo and Dilcher, 2001; Saxena and Trivedi, 2009; Jardine, 2011). All pollen grains from Kalewa were counted using a LEICA DM LB2 LM, and a Zeiss Axiophot Microscope at the Institute for Biodiversity and Ecosystem Dynamics (IBED). Pollen count data are shown in Supplementary Data (Table S1). Pollen diagrams were made in Tilia 2.1.1 (Grimm, 1991) with cluster analysis program CONISS (Grimm, 1987).

LM micrographs were produced with a FUJIFILM X-M1 digital camera (Fujifilm Holdings Corporation, Tokyo, Japan) connected with a Zeiss Axiophot Microscope (Carl Zeiss, Oberkochen, Germany) under the 630× magnification (with oil) at the IBED. We also investigated the morphological details of the sporomorphs under a JEOL JSM·6400 SEM at the DoP, with the single-grain analysis method (Zetter, 1989; Halbritter et al., 2018). The micrographs were then processed in the software CorelDRAW 2019 (Corel Corporation, Ottawa, Canada). Each palynomorph under LM/SEM in Figs. 4 and 5 was referenced with sample number, residue number, and the “England Finder” coordinates if applicable (Supplementary Data, Table S2).

3.4. Sequence biostratigraphy

Depositional sequences can be identified from the examination of microfossil distribution patterns, which is termed sequence biostratigraphy. This method was developed using foraminifera and nannofossils by Armentrout (1991, 1996) and Shaffer (1987) and extended to consider palynomorph distributions by Morley (1996) and Morley et al. (2021). In this study, systems tracts were suggested based on palynomorph assemblages. They were then dated using the magnetostratigraphy for the succession as established by Westerweel et al. (2020). The succession of depositional sequences was then compared to the predicted succession for the late Eocene from the ICS website (ICS, 2020) which is a modification of the scheme of Hardenbol et al. (1998).

3.5. Bioclimatic analysis

We applied bioclimatic analysis (BA, e.g., Kershaw and Nix, 1988; Kershaw, 1997; Reichgelt et al., 2013) to quantitatively derive the paleoclimatic information from Yaw Formation data. BA is a method that compares the mutual climate range (MCR), using the climatic envelope of the nearest living relatives (NLRs) from fossil taxa to derive the climate ranges in which the majority of an assemblage could co-occur (e.g., Kershaw, 1997; Eldrett et al., 2009; Thompson et al., 2012; Reichgelt et al., 2013). The method has been extensively used to reconstruct the climate in the Eocene (e.g., Eldrett et al., 2009; Greenwood et al., 2010; Pross et al., 2012; Willard et al., 2019), and even the Cretaceous (e.g., Klages et al., 2020). BA is slightly different from the coexistence approach (CoA, Mosbrugger and Utescher, 1997) in terms of how climatic range of each taxon is determined: BA defines the overlapping zone based on the 10th and 90th percentiles to exclude climatic outliers (Greenwood et al., 2003, 2005). In our study, we identified the pollen types (method refers to 3.3) and based on this suggested their NLRs (modern family, genus or species; botanical affinities in Huang et al., 2021); we then obtained the climatic envelopes with the occurrence data of these NLRs. The co-occurred mutual climate ranges of different climatic variables of the NLRs thus can reflect the climatic conditions of the fossil pollen types observed from the Yaw Formation.

Anemophilous taxa are mostly widely dispersed; including pollen types in low percentages derived from anemophilous taxa, particularly those from the mountain areas, can mislead the interpretation of the climate near the accumulation site. Therefore, they were removed in the BA when their percentages were smaller than a threshold, as they were likely blown in from a distant locality (e.g., Li et al., 2015; Tang et al., 2020). We followed Li et al. (2015) which referred to some previous quantitative studies on the relationship between modern pollen in surface samples and vegetation (e.g., Xu et al., 2007), to remove some anemophilous taxa. This procedure was applied to *Pinus* and *Betula* pollen types, which are less than 25% and 4% respectively. We also excluded *Alnus*, *Carpinus*, *Juglans* and *Taxodium* pollen types, while the former three were with percentages less than 4%, and the latter one less than 2%. Local elements such as algae, aquatics (*Myriophyllum*, *Jussiaea* and Liliaceae types) and xerophytic taxa (*Ephedra* types) were also excluded from the analysis, as they may also confound the paleoclimatic interpretations.

Occurrence data of the NLRs were obtained from the Global Biodiversity Information Facility (GBIF, www.gbif.org). These data were processed to delete duplicated and misplaced points following the methods of Palazzesi et al. (2014) and Zizka et al. (2019). Corresponding climate variables were extracted from the WorldClim Version 2 (https://worldclim.org/version2, 30 seconds in resolution). The modern climate variables in the study area were also derived from WorldClim Version 2 with a resolution of 30 seconds. As currently Kalewa is located at a different latitude (Fig. 1b; *c*. 23° N) from the Eocene (Fig. 1c; *c*. 5° N; Westerweel et al., 2020), the modern

climate variables were also derived from the Phiman area (Fig. 1b; 6°37′ N, 100°4′ E) in Thailand for comparison. Like for the Eocene Burma Terrane, the Phiman area is located on the eastern shorelines of the broader Bengal Bay and is close to the equator. The Phiman area is located near sea level, has a deltaic environment and a unique monsoonal rainy season in summer.

We estimated 11 quantitative climatic variables: (a) temperature (°C) including mean annual temperature (MAT), maximum temperature of warmest month (MTWM), minimum temperature of coldest month (MTCM), mean temperature of warmest quarter (MTWQ), and mean temperature of coldest quarter (MTCQ); (b) precipitation (mm) including mean annual precipitation (MAP), precipitation of wettest month (PWETM), precipitation of driest month (PDRYM), precipitation of wettest quarter (PWETQ), and precipitation of driest quarter (PDRYQ); and (c) monsoon intensity index (MSI). The MSI was calculated based on precipitation variables with the equation of Li et al. (2015), a modified version of van Dam (2006) and Xing et al. (2012): MSI = (PWETM–PDRYM)/MAP × 100. Therefore, it indicates seasonality in precipitation, with high PWETM usually indicating higher seasonality (van Dam, 2006). To our knowledge, this is the first time that BA is applied on paleovegetation datasets from SE Asia.

3.6. Rarefaction on sporomorphs diversity

We compared the sporomorph diversity in the Yaw Formation with middle to late Eocene palynofloras from four sites that were formed in depositional systems comparable to the studied sediments in Kalewa (for the locations of the three Asian sites, see Fig. 2a). Sample information and palynological data for the four sites and Kalewa site can be found in Supplementary Data (Tables S3–S7).

The depositional environments and vegetation types of the four sites can be summarized as follows: (a) The late Eocene Kopili Formation in North Cachar Hills, Assam, India, was deposited in coastal and freshwater swamps and ponds (Saxena and Trivedi, 2009). The flora is characterized by a tropical-subtropical, warm-humid climate with heavy precipitation. Pteridophytes, mangroves and other coastal elements such as palms, predominate in these sediments; (b) The middle to late Eocene Nanggulan Formation from the Watupuru River, central Java, Indonesia, was deposited in a transgressive succession and containing rich and diverse sporomorphs (Lelono, 2000); (c) The Zhenjiang section in Maoming Basin, Guangdong, China includes the Youganwo and Huangniuling formations (Aleksandrova et al., 2015). The late Bartonian Youganwo Formation was deposited in swampy floodplains and freshwater lakes, favoring the development of unseasonal wet subtropical forests with evergreen taxa. The Priabonian Huangniuling Formation was deposited in a broad floodplain bearing seasonal tropical forests; (d) The selected sites in Colombia are situated in the Catatumbo and eastern Cordillera-Llanos foothill basins, where sediments accumulated in a fluvial or coastal plain setting (with samples from *c.* 38–36 Ma time interval) (Jaramillo et al., 2006).

For application of the rarefaction method (e.g., Birks and Line, 1992) to determine sporomorph diversity, we refer to Jardine et al. (2018). We included all the sporomorphs we identified from the section (including the anemophilous taxa and local elements which were excluded in bioclimatic analysis), following previous studies (e.g., Jaramillo et al., 2006, 2010; Jardine et al., 2018). Taxonomic richness (number of sporomorphs) was standardized on both coverage and sample size by unified interpolation and extrapolation (Chao and Jost, 2012; Colwell et al., 2012). Expected richness was calculated using abundance data within samples and using incidence data from pooled samples within geologic ages (Gotelli and Colwell, 2001). For within-sample richness, a coverage level of 0.8 was calculated to include most samples in the sections. Expected richness at the coverage level of 0.9 and sample sizes of 160 and 220 was also applied to explore the impact of coverage versus sample size. For within-age richness, we pooled within-sampling localities without the impact of the different geographic extent. We assessed within-sample evenness (a parameter indicating relative abundances of the various sporomorphs in a sample) through the time series with the E_{var} evenness metric of Smith and Wilson (1996). The Chao1 richness estimator was used to estimate total richness (Chao and Jost, 2012). R v.3.6.1 (R Core team, 2019) was used to perform diversity rarefaction (sampling standardization and Chao1 metric calculation) with the iNEXT package (Hsieh et al., 2014).

4. Results and interpretation

4.1. Age of the Yaw Formation and correction of age of palynological zonation

The age of our section is 38.4–37 Ma obtained by magnetostratigraphy and geochronology (Licht et al., 2019; Westerweel et al., 2020). However, the presence of *Proxapertites operculatus* and *Meyeripollis naharkotensis* and the absence of *Magnastriatites howardi* throughout the succession is indicative of palynological zone E8, when using the SE Asian palynological zonation scheme presented in van Gorsel et al. (2014) and recently updated in Morley (2020). The E8 zone was interpreted to be of late Eocene age and ranging from 36 Ma to 35 Ma, based on long-ranging larger foraminifera and regional correlation (Pieters et al., 1987). This suggests that the age of zone E8 needs to be adjusted and extended deeper into the late Eocene.

4.2. Vegetation dynamics reconstructed from quantitative palynological analysis

The late Eocene Kalewa sedimentary record yielded more than 141 sporomorph types (Huang et al., 2021). Characteristic sporomorphs are shown in Figs. 4 and 5, with numbers of sample/residue and England Finder positions shown in Supplementary Data (Table S2). From the spatial perspective, the 141 sporomorph types were derived from plant taxa growing in mangroves/back-mangroves and coastal forests in the lower deltaic plain; swamp forests along

rivers, with herbaceous swamps and marshes, possibly associated with floodplain lakes, and gallery forests in the upper deltaic plain; perhumid/wet, evergreen, seasonally dry forests, and piedmont and montane forests, from a swampy coastal setting to dry *terra firma* (i.e., the range of habitats of well-drained, non-swamp soils that constitute the hinterland) forests in the upstream area (Huang et al., 2021). Pollen diagrams are presented in Figs. 6 and 7 and are divided into the following six pollen zones (K1–6) (Table 1) which are thought to reflect vegetation changes based on visual observation coupled with cluster analysis.

4.3. Bioclimatic analysis of the sporomorph assemblage

The results from bioclimatic analysis are based on 11 climatic variables of the Kalewa section and are shown in Table 2 and Supplementary Data (Figs. S1–S10), including the present climate variables in Kalewa and Phiman areas. MAT is higher than the modern-day level of Kalewa area and lower than that of Phiman area, while MAP is similar to that of Kalewa area and lower than that of Phiman area. Compared with the modern-day Kalewa area, maximum temperature of warmest month, mean temperature of warmest quarter, precipitation of wettest month, precipitation of wettest quarter, and monsoon intensity index are lower, while minimum temperature of coldest month, mean temperature of coldest quarter, precipitation of driest month, and precipitation of driest quarter are higher; compared with the modern-day Phiman area, maximum temperature of warmest month, minimum temperature of coldest month, mean temperature of coldest quarter, mean temperature of warmest quarter, precipitation of wettest month, and precipitation of wettest quarter are lower, while precipitation of driest month, precipitation of driest quarter, and monsoon intensity index are higher.

Bioclimatic analysis results for each sample were shown in Supplementary Data (Table S8) and Fig. 8, suggesting three 'dry-wet' climatic cycles from the bottom to the top of the section. These cycles are also clearly displayed from the examination of groupings within the *terra firma* pollen component, which shows that intervals with a drier climate are indicated by maxima of 'seasonally dry trees and shrubs' which correspond to maxima of deciduous montane trees (Fig. 7).

4.4. Palynological diversity in the middle to late Eocene tropics

Within-sample richness (Fig. 9) in the Nanggulan Formation (central Java, Indonesia) is highest, while that in Yaw Formation (central Myanmar) is the second highest and similar to the sediments in the Catatumbo and eastern Cordillera-Llanos foothill basins (Colombia). Within-sample richness in the three aforementioned geological units are higher than that in the Kopili Formation (Assam, India), and Zhenjiang section (Guangdong, China). The four geological units except the sediments in the Catatumbo and eastern Cordillera-Llanos foothill basins (Colombia),

have a positive correlation between richness and evenness, while the sediments in Colombia has a very low and non-richness-correlated evenness.

In the Yaw Formation (central Myanmar), there is a positive correlation between evenness and expected richness. Yet this is less pronounced with Chao1 estimated richness. In the Kopili Formation (Assam, India) and Nanggulan Formation (central Java, Indonesia), evenness correlates also with expected richness and Chao1 estimated richness, though they do not show any noticeable change throughout the section. In the Zhenjiang section (Guangdong, China), expected richness is higher at the bottom; Evenness correlates more with Chao1 estimated richness than with expected richness, and does not show any clear change throughout the section. In the sediments in Colombia, richness and evenness do not correlate; evenness in all samples is low and almost has no variation.

Within-sample diversity results are provided in Supplementary Data (Figs. S11–S25 and Tables S9–S13) and Fig. 9. Some of the confidence intervals on the Chao1 estimated richness are very large and not displayed in Fig. 9, and included in Supplementary Data (Figs. S11, S14, S17, S20 and S23) that shows the large confidence intervals are tied to count size. When the count size increases, Chao1 estimated richness increases and the confidence intervals become larger. When constructing the richness and evenness at different levels, both for coverage and for the sample-size based richness, they show similar results (Supplementary Data, Figs. S12, S15, S18 and S21).

4.5. Sequence biostratigraphic evaluation

A simple landscape model for the Yaw Formation was proposed by Huang et al. (2021) based on the presence of palynomorph indicators of the major biomes for the late Eocene CMB. Here we look at evidence for vertical changes in sporomorph assemblages and determine whether these may be interpreted in terms of temporal changes in vegetation, and discuss the possibility that these changes may relate to changing sea level and climate. The Yaw palynological succession suggests varying vegetation changes, with periods of increased perhumid taxa during warmer/wetter periods and increased seasonally dry and montane taxa during cooler/drier intervals. There is also a close relationship between the abundance of mangrove/back-mangrove elements, the features of the swamp vegetation, and periods of warmer/wetter climate. For instance, the warmer/wetter period of zone K2 coincides with mangrove pollen maximum and a maximum of *Dicolpopollis* spp., whereas zone K6, which was similarly warm and wet, exhibits a maximum of *Dicolpopollis* spp. without mangroves elements, probably due to a more proximal depositional setting, although it does contain rare chitinous foraminiferal test linings, indicating marine influence. The synchronicity of a period of warmer climate coupled with a mangrove pollen maximum suggests that eustasy may be driving the recorded vegetation changes and that the assemblages may be reflecting systems tracts (Morley, 1996; Morley et al., 2021). However, the Yaw succession is characterized by extremely high sediment accumulation rates and high

subsidence (*c*. 1 km/Myr), and since facies throughout the succession are all contained within a narrow range in a coastal plain setting (Licht et al., 2019), it is possible that slight variations in relative sea level were driven by changes in the rate of subsidence or sediment supply.

The Mahakam Delta, within the Kutei Basin on the east coast of Borneo (Fig. 1b) in Indonesia provides an excellent analogue for examining the architecture of systems tracts and their biostratigraphic response in an area of similarly very high rates of subsidence and sediment supply (Morley et al., 2004; Saller et al., 2004; Morley and Morley, 2010). There, depositional cycles are dominated by progradational packages deposited during highstands and falling eustatic sea level separated by repeated thin carbonate beds. Thus, both highstand and lowstand sediments may be sequestered on the shelf, but a carbonate bed formed at times of rapid sea level rise and comprises the transgressive systems tract. The Kutei Basin sequence follows the "Galloway" sequence model (Galloway, 1989), and despite the rapid subsidence, phases of eustatic sea level rise are clearly reflected in the sedimentary succession, in line with the suggestion of Miller et al. (2011) who emphasized that eustatic and tectonic processes occur at different timescales. In the Kutei Basin, periods of rapid sea level rise are reflected by maxima of mangrove pollen, with warmer and/or wetter climates during the highstand (Morley et al., 2004; Morley and Morley, 2010). It is therefore justified to examine the Yaw succession for mangrove pollen maxima coinciding with phases of ameliorating climate to differentiate sedimentary packages that may reflect systems tracts following the model of Morley et al. (2021).

The succession represented by zone K1, where assemblages suggest a seasonally dry climate, and cooler temperatures, are consistent with late highstand (HST) or lowstand (LST) deposition. For zone K2, assemblages suggest a wetter and warmer climate, and increased mangrove pollen indicates increased marine influence, which is consistent with deposition in a more aggradational setting within the transgressive systems tract (TST). For the succession spanning zones K3, K4 and K5, most assemblages suggest a slightly drier and cooler climate, and mangrove pollen reaches a minimum, which is consistent with deposition in a prograding HST setting. The youngest interval, represented by zone K6, yielded assemblages suggesting a warmer and wetter climate, and common *Dicolpopollis kalewensis*, and shows similarities with zone K2. It does not contain common mangrove pollen but does include rare chitinous foraminiferal test linings. This interval is consistent with a facies and climatic setting similar to K2, but in a more proximal setting due to the reduced mangrove pollen recovery. This package is therefore consistent with proximal deposition within the TST. The systems tract succession is summarized in Fig. 10.

The age of the Yaw succession has been accurately determined from U–Pb zircon dating (Licht et al., 2019), magnetostratigraphy, U–Pb apatite dating and apatite fission track dating (Westerweel et al., 2020). The magnetostratigraphic dating can be used to provide approximate dates in Ma for each of the pollen zone boundaries, and the age of systems tract boundaries. The age of the succession of systems tracts has been compared with the age of late Eocene sequences

using the ExxonMobil model (Hardenbol et al., 1998), taken from the ICS TimeScale Creator website (ICS, 2020) in Fig. 11.

Remarkably, there is a close relationship between the timing of the proposed transgressive systems tracts, and stratal surfaces shown in two of the late Eocene sequences by Hardenbol et al. (1998). Firstly, the upper boundary of zone K2, suggested to reflect a TST, would form the maximum flooding surface, or MFS, of its contained sequence, and is dated at 38.05 Ma based on magnetostratigraphy, and compares favorably with the maximum flood of Sequence PaBart-1 of Hardenbol et al. (1998), dated at 38.2 Ma. Secondly, the upper boundary of zone K6, also interpreted as a TST, is dated at 37.1 Ma based on magnetostratigraphy, and ties closely with the MFS of Sequence PaPr-1 of Hardenbol et al. (1998), also dated at 37.1 Ma. The latter, however, must be considered a minimum date, as the upper boundary of zone 6 corresponds to the top of the Yaw Formation, which is an erosional surface, and some of the interval may have been removed by erosion.

The pattern of climate and relative sea level changes seen in the Yaw succession and their magnetostratigraphic framework are consistent with a correlation to sequences PaBart-1 and PaPr-1 (Fig. 11). Zone K1, reflecting a period of drier climate, is correlated with the PaBart-1 lowstand, the two TSTs relate to periods of wetter climate, and zone K5 is correlated the lowstand (LST) of Sequence PaPr-1.

5. Discussion

5.1. Landscape model and temporal vegetation change

By evaluating the palynological record within the framework of the succession of systems tracts, the vegetation on the deltaic plain and in the hinterland can be more easily visualized (Figs. 10 and 12). The pollen zones K1–6 (i.e., temporal trends) are discussed below.

The lowstand deposits represented by zone K1, in a seaward position on a prograding delta plain explaining the presence of just limited mangroves, together with swamp forest, with *Alchornea* and herbaceous fern swamps, and the climate at the time would have been the driest of the whole formation, with lowland *terra firma* vegetation including *Pinus*, suggestive of some vegetation types in central Thailand today (Ratnam et al., 2016). Myrtaceae pollen is common in this interval and could have been derived from either *terra firma* or swamp trees.

Then, with rising sea levels reflected by pollen zone K2, mangroves would have been well represented, and with a change to a wetter climate, rattan swamps, reflected by a maximum of *Dicolpopollis kalewensis*, would have been extensive on the aggrading coastal plain. The swamp vegetation would also have included common *Campnosperma* and *Mischocarpus*, together with the parent plant of *Longapertites* spp. (possibly *Eugeissona*), the parent plant of *Palmaepollenites kutchensis* and the climbing fern *Stenochlaena palustris,* and also hornworts, such as *Phaeoceros.*

The presence of undifferentiated palm (i.e., "Other palms' in Fig. 6) pollen suggest that Arecaceae would also have been prominent elements of the vegetation. Moreover, the very little pollen from seasonally dry vegetation indicates that this zone was the period of wettest climate in the section. In this succession, montane pollen is at a minimum, and this would be consistent with warmer climates, with montane vegetation occurring at higher altitudes in upland areas and with reduced areal representation.

Highstand delta progradation reflected by the zone K3 succession, with stabilized sea levels and a change to a slightly drier climate resulted in the reduction of mangrove swamps (although locally tidal channels could have intermittently brought mangrove pollen into the delta plain) and a change to fern-dominated swamps on the delta plain, which were later replaced by swamps dominated by the parent plant of *Meyeripollis naharkotensis*. The initial stage of swamp development with abundant fern swamps also saw a return of *Alchornea*, and *Palaquium* could also have been a significant component of swamp vegetation. In the hinterland, drier climates resulted in the expansion of taxa from seasonally dry forests such as Caesalpinioideae, indicated by the presence of *Margocolporites* spp., and also *Berlinia*. Montane pollen shows a distinct increase in abundance, and mainly consists of evergreen elements, with *Engelhardia* and Magnoliaceae, and this could reflect the expansion of montane vegetation, with cooler climates with montane forests occurring at lower altitudes.

The subsequent stage of development of the succession, reflected by assemblages within zones K4–5, included widespread swamps with the parent plant of *Meyeripollis naharkotensis*, which also bore common *Campnosperma* and *Mischocarpus* and herbaceous swamps with hornworts, such as *Phaeoceros*. In zone K5, *Terra firma* vegetation was characterized by evergreen forests with widespread Sapotaceae, and a slight increase in seasonally dry climate elements such as *Austrobuxus*, Caesalpinioideae, *Berlinia* and *Pinus* suggesting a drier climate, possibly reflect a 'lowstand' phase. With respect to montane vegetation, this interval is characterized by regular pollen of deciduous angiosperms, such as *Juglans* and *Carpinus*.

The final stage of development of the Yaw succession was a further change to more transgressive conditions and a wetter climate with the TST reflected by palynomorph assemblages within zone K6. This again resulted in the widespread establishment of rattan swamps on the delta plain, indicated by a further maximum of *Dicolpopollis kalewensis*. However, the delta had prograded sufficiently that by this time deposition was beyond the reach of brackish influence, and so there were no mangrove swamps at the sampled locality, although rare chitinous foraminiferal test linings were noted. Swamp vegetation also included *Palaquium* and the parent plant of *Meyeripollis naharkotensis*, as well as an Areceae (Arecaceae) taxon, which produced *Palmaepollenites kutchensis*. The climate would have been wet, since dry climate elements are missing, and pollen of montane taxa is rare, suggesting that montane vegetation may have been of reduced extent compared to the cooler and drier periods of the earlier possible LST and HST successions. It is of interest that despite the perhumid climate, fern spores are less frequent than

within the underlying succession. This may indicate that swamps during this period were relatively closed, and that the niche available for fern swamps was reduced.

5.2. A unique proto-monsoonal climate in the late Eocene CMB

The abundance of *terra firma* taxa such as the parent plants of *Anacolosidites*, *Meyeripollis naharkotensis*, *Palmaepollenites kutchensis* and diverse Sapotaceae, suggest a seasonally wet/perhumid climate (Huang et al., 2021). The parent plants of *Malvacidites* ?*diversus* and *Pinus* occur in seasonally dry climatic conditions, away from riparian areas. Therefore, we propose that seasonal evergreen forests dominated the *terra firma* areas with perhumid vegetation in areas of alluvial swamps, and with drier areas supporting seasonally dry, semi-evergreen and deciduous forests. This vegetation pattern is typical to what is found around the Bay of Bengal today and support a monsoon-like climate at the time of the Yaw Formation, supporting the existence of proto-monsoons in the middle to late Eocene of Asia (e.g., Licht et al., 2014; Su et al., 2020). When compared with the Phiman area (at the same latitude today), the late Eocene CMB is drier, with at least 400 mm less annual rainfall. The late Eocene monsoon intensity index (14–15) is higher than today at the same latitude (13 in Phiman), but lower than at its present-day location (20 in Kalewa). The lower rainfall and higher monsoonal index in the Eocene compared to today, at the same latitude near the equator, corroborate a well-marked seasonal migration of the Intertropical Convergence Zone (ITCZ; Spicer et al., 2017). Our data thus confirm the existence of wide ITCZ migrations during the Eocene that provide a mechanism for proto-monsoonal rainfall (Farnsworth et al., 2019; Tardif et al., 2021).

The late Eocene CMB had a cooler (at least 2 °C lower) climate than today as a similar latitude, as suggested by the reconstructed MAT (Table 2; Supplementary Data, Fig. S1). Cool (near-)equatorial temperatures in the Eocene have also reported from India (e.g., early Eocene; Shukla et al., 2014; Bhatia et al., 2021) and Asian mid-tropics (e.g., middle Eocene; Spicer et al., 2014). Previous authors have suggested that these cooler temperatures reflect a significant poleward heat transport during the Eocene greenhouse world (Shukla et al., 2014; Spicer et al., 2014). Warmer temperatures are found in the middle Eocene of central Myanmar, in the earlier Pondaung Formation, via the study of fossil wood anatomy (MAT = 30 °C (± 2 to 5 °C); Licht et al., 2015) and body size of fossil squamates (MAT > 27 °C, Head et al., 2013). The Pondaung Formation was deposited at the end of the Middle Eocene Climatic Optimum (MECO; Licht et al., 2015), the most noticeable short-lived warming event in the middle Eocene (Bohaty and Zachos, 2003), potentially explaining warmer temperatures. However, geochemical proxies yield warmer, not cooler near-equatorial surface temperatures globally (e.g., Peason et al., 2001; Keating-Bitonti et al., 2011; van Dijk et al., 2020), raising doubts about the accuracy of paleobotanical temperature estimates.

We see four possible explanations in the Eocene cooler temperatures found in the monsoonal domain: (1) Mis-identification of the NLRs of fossil taxa can introduce errors in climate reconstructions; this mechanism could explain our results, obtained with BA, but does not explain cooler temperatures found with morphological methods that do not rely on the NLRs (e.g., CLAMP; Shukla et al., 2014; Spicer et al., 2014; Bhatia et al., 2021); (2) The botanical database on which climatic parameters are extracted is incomplete (GBIF database for BA), and do not contain enough occurrences to fully cover the entire monsoonal domain; this explanation stands for the GBIF database but not for CLAMP approaches, that have been calibrated with many monsoonal stations (e.g., Spicer et al., 2014); (3) Extant taxa adapted to monsoonal climates are fundamentally different to fossil ones, and there is no modern botanical analogues to Eocene monsoonal climates; this explanation is particularly justified as warm equatorial temperatures such as seen in Eocene climate simulations (e.g., Zhu et al., 2019) and benthic data (Westerhold et al., 2020) have not been reached since the fall into the Oligocene coolhouse; (4) As previous study (Spicer et al., 2011) suggests, effects of evapotranspirational cooling of canopy can lead to comparatively cooler climates for CLAMP analysis. We thus postulate that the unique monsoonal climate and ecosystems of the Eocene Bengal Bay, driven by warm temperatures and ITCZ migration, have no good modern analogue, which result in poor paleo-temperature reconstructions.

5.3. Plant diversity in the late Eocene tropics

The five localities of middle to late Eocene age that we compared in this study were all situated in the tropics, with deposition in fluvial or coastal plain settings. In terms of forest composition and depositional environments, the Yaw Formation (central Myanmar) best resembles the Kopili Formation (Assam, India), as they are both dominated by seasonal evergreen forest elements, bear the same conifers (e.g., *Pinuspollenites*) and show a dominance of pteridophytic spores (Saxena and Trivedi, 2009; Huang et al., 2020, 2021). Both geological units were deposited in coastal settings, and were likely just a few hundreds of kilometers apart along the shorelines of the Bengal Bay.

Our results suggest that the within-sample richness in the Watupuru section (central Java, Indonesia) is the highest among the five sites, though the richness of the Kopili Formation (Assam, India), the Zhenjiang section (Guangdong, China), and the sediments in the Catatumbo and eastern Cordillera-Llanos foothill basins (Colombia) may be biased due to limited sampling (Supplementary Data, Figs. S16, S19 and S22). The rarefaction curve in the Yaw Formation (central Myanmar) indicates that overall, the sampling is complete enough (Supplementary Data, Fig. S13), which means adding more samples would not add significantly more species.

The highest species richness of the Nanggulan Formation in the Watupuru section (central Java, Indonesia) is attributed to its near-equatorial position and perhumid (perennially wet)

climate at that time (Morley, 2000). The species richness of the Yaw Formation comes second; this lower diversity might be explained by slightly higher latitudes for the Eocene Burma Terrane than the for the Watupuru section (Westerweel et al., 2019), or by the more pronounced monsoonal climate with well-marked seasonality on the Burma Terrane. The difference in species richness between the Kopili Formation and the Yaw Formation, despite similar paleolatitudes, might reflect the higher connectivity of the Burma Terrane during the Eocene. The Burma Terrane, located at the edge of India and Asia at that time, acted as a crossroads for plant dispersals (Huang et al., 2021), and this crossroads may have persisted until the present day, and makes Myanmar range among the most important biodiversity hotspots at a global scale (Myers et al., 2000) with *c.* 12,340 species of spermatophytes (based on Kress et al., 2003; Yang et al., 2020).

6. Conclusions

In this study, we investigated the vegetation and climate history of the late Eocene Yaw Formation in the Central Myanmar Basins, by quantitatively analyzing changes in sporomorph composition. We also evaluated the change of depositional environments in a sequence biostratigraphic framework and floristic diversity with rarefaction analysis. We conclude that:

(1) Changes of vegetation and depositional environments are evaluated within the framework of two transgressive-regressive depositional successions, and three wet-dry climate cycles. The late Eocene Kalewa region was characterized by lowland evergreen forests, due to its near-equatorial and coastal plain position. The vegetation was evaluated within a framework of, six pollen zones, which were characterized by fern and *Alchornea* swamps, *Proxapertites* mangroves and rattan swamps, fern swamps, *Meyeripollis* swamps, and rattan swamps from the bottom to the top of the section. The succession was evaluated from a sequence biostratigraphic perspective that allowed vegetation change to be visualized within the dynamic perspective of transgressions and regressions driven by sea level change. During times of rising sea levels, the climate was wetter, and coastal vegetation communities extended further landward, whereas during periods of sea level stillstand, and subsequent fall, the climate was drier and deltas prograded seaward, resulting in the presence of more fluvial facies at the depositional locality.

(2) Bioclimatic analysis indicates that in the late Eocene, the CMB was drier (mean annual precipitation = 1635–1637 mm), and cooler (mean annual temperature = 25.4–25.6 °C), with similar seasonality (monsoon intensity index = 14–15) than/as in the present day at the same near-equatorial latitude (*c.* 6° N; mean annual precipitation = 2053 mm, mean annual temperature = 27.6 °C, monsoon intensity index = 13). Presence and abundance of diagnostic taxa indicate a seasonally dry, monsoonal climate, though with more evenly distributed rainfall than today. These results corroborate the presence of Eocene proto-monsoons driven by a seasonal ITCZ migration; we suggest that cooler temperatures may be due to the lack of adequate modern analogues for the Eocene monsoonal climate of the Bengal Bay.

(3) Rarefaction analysis performed on five Eocene tropical sites in terms of within-sample richness, evenness, and coverage and sample size-based interpolation and extrapolation suggests high species richness for the Yaw Formation compared to other sites, though lower than the near-equatorial Nanggulan Formation in central Java, with a wetter climate. The high floristic diversity of the Yaw Formation is likely enhanced by its near-equatorial location, at the crossroads for plant dispersals between India and Asia.

Taken together, we suggested that the proto-monsoonal climate and tectonics (e.g., the plate collision and paleogeography) had shaped the vegetation, depositional environments, and floristic diversity in the late Eocene of central Myanmar.

Acknowledgements

We are indebted to all members of the Myanmar Paleoclimate and Geodynamics research group for sample collection. We thank Annemarie Philip and Malcolm Jones for processing palynological samples; Friðgeir Grímsson and Reinhard Zetter for assistance on microphotography and identification of palynomorphs; Shufeng Li and He Tang for help on bioclimatic analysis; Phillip Jardine for support on rarefaction analysis and helpful comments on an initial draft. We also thank the two anonymous reviewers for their constructive comments that helped us to improve the manuscript. H.H. was supported by the China Scholarship Council (CSC grant 201604910677) and the University of Amsterdam; A.L., G.D.-N., and J.W. acknowledge the European Research Council Consolidator Grant (MAGIC 649081); A.L. was additionally funded by the ANR grant ANR-19-ERC7-0007.

Supplementary data to this article can be found online at XXXX

References

Aleksandrova, G.N., Kodrul, T.M., Jin, J.H., 2015. Palynological and paleobotanical investigations of Paleogene sections in the Maoming Basin, South China. Stratigr. Geol. Correl. 23, 300–325.

Armentrout, J.M., 1991. Paleontologic constraints on depositional modelling: Examples of integration of biostratigraphy and seismic stratigraphy, Gulf of Mexico. In: Weimer, P., Link, M.H. (Eds.), Seismic Facies and Sedimentary Processes of Submarine Fans and Turbidite Systems. Frontiers in Sedimentary Geology Series Springer, New York, USA, pp. 137–170.

Armentrout, J.M., 1996. High resolution sequence biostratigraphy: example from the Gulf of Mexico Plio-Pleistocene. In: Howell, J.A., Aitken, J.F. (Eds.), High Resolution Sequence Stratigraphy: Innovations and Applications. Geological Society, London, Special Publications 104, UK, pp. 65–86.

Ashok, K., Guan, Z., Saji, N., Yamagata, T., 2010. Individual and combined influences of ENSO and the Indian Ocean dipole on the Indian summer monsoon. J. Climate 17, 3141–3155.

Ashton, P., 2014. On the Forests of Tropical Asia: Lest the Memory Fade. Kew Publishing, London, UK.

Beck, H.E., Zimmermann, N.E., McVicar, T.R., Vergopolan, N., Berg, A., Wood, E.F., 2018. Present and future Köppen-Geiger climate classification maps at 1-km resolution. Sci. Data 5, 180214.

Bhatia, H., Khan, M.A., Srivastava, G., Hazra, T., Spicer, R.A., Hazra, M., Mehrotra, R.C., Spicer, T.E.V., Bera, S., Roy, K., 2021. Late Cretaceous–Paleogene Indian Monsoon climate vis-à-vis movement of the Indian plate, and the birth of the South Asian Monsoon. Gondwana Res. 93, 89–100.

Bhatia, H., Srivastava, G., Spicer, R.A., Farnsworth, A., Spicer, T.E.V., Mehrotra, R.C., Paudayal, K.N., Valdes, P., 2021. Leaf physiognomy records the Miocene intensification of the south Asia monsoon. Glob. Planet. Change 196, 103365.

Birks, H.J.B., Line, J.M., 1992. The use of rarefaction analysis for estimating palynological richness from Quaternary pollen-analytical data. The Holocene 2, 1–10.

Bohaty, S.M., Zachos, J.C., 2003. Significant Southern Ocean warming event in the late Middle Eocene. Geology 31, 1017–1020.

Boos, W., Kuang, Z., 2010. Dominant control of the South Asian monsoon by orographic insulation versus plateau heating. Nature 463, 218–222.

Chao, A., Jost, L., 2012. Coverage-based rarefaction and extrapolation: standardizing samples by completeness rather than size. Ecology 93, 2533–2547.

Clift, P.D., Hodges, K.V., Heslop, D., Hannigan, R., Van Long, H., Calves, G., 2008. Correlation of Himalayan exhumation rates and Asian monsoon intensity. Nat. Geosci. 1, 875–880.

Colwell, R.K., Chao, A., Gotelli, N.J., Lin, S.Y., Mao, C.X., Chazdon, R.L., Longino, J.T., 2012. Models and estimators linking individual-based and sample-based rarefaction, extrapolation, and comparison of assemblages. J. Plant Ecol. 5, 3–21.

de Terra, H., 1944. Component geographic factors of the natural regions of Burma. Ann. Am. Assoc. Geogr. 34, 67–96.

Ding, L., Spicer, R.A.,Yang, J., Xu, Q., Cai, F., Lai, Q., Wang, H, Spicer, T.E.V., Yue, Y., Shukla, A., Srivastava, G., Khan, M.A., Bera, S., Mehrotra, R., 2017. Quantifying the rise of the Himalaya orogen and implications for the South Asian monsoon. Geology 45, 215–218.

Eldrett, J.S., Greenwood, D.R., Harding, I.C., Huber, M., 2009. Increased seasonality through the Eocene to Oligocene transition in northern high latitudes. Nature 459, 969–973.

Farnsworth, A., Lunt, D.J., Robinson, S.A., Valdes, P.J., Roberts, W.H., Clift, P.D., Markwick, P., Su, T., Wrobel, N., Bragg, F., Kelland, S.J., Pancost, R.D., 2019. Past East Asian monsoon evolution controlled by paleogeography, not CO_2. Sci. Adv. 5, eaax1697.

Galloway, W.E., 1989. Genetic stratigraphic sequences in basin analysis I: architecture and genesis of flooding-surface bounded depositional units. AAPG Bull. 73, 125–142.

Germeraad, J.H., Hopping, C.A., Muller, J., 1968. Palynology of Tertiary sediments from tropical areas. Rev. Palaeobot. Palynol. 6, 189–348.

Gotelli, N., Colwell, R.K., 2001. Quantifying biodiversity: procedures and pitfalls in the measurement and comparison of species richness. Ecol. Lett. 4, 379–391.

Greenwood, D.R., Archibald, S.B., Mathewes, R.W., Moss, P.T., 2005. Fossil biotas from the Okanagan Highlands, southern British Columbia and northeastern Washington State: climates and ecosystems across an Eocene landscape. Can. J. Earth Sci. 42, 167–185.

Greenwood, D.R., Basinger, J.F., Smith, R.Y., 2010. How wet was the Arctic Eocene rain forest? Estimates of precipitation from Paleogene Arctic macrofloras. Geology 38, 15–18.

Greenwood, D.R., Moss, P.T., Rowett, A.I., Vadala, A.J., Keefe, R.L., 2003. Plant communities and climate change in southeastern Australia during the early Paleogene. Spec. Pap. Geol. Soc. Am. 369, 365–380.

Grimm, E.C., 1987. CONISS: a FORTRAN 77 program for stratigraphically constrained cluster analyses by the method of incremental sum of squares. Comput. Geosci. UK 13 (1), 13–35.

Grimm, E.C., 1991. Tilia and Tiliagraph. Springfield, Illinois State Museum.Guo, Z.T., Ruddiman, W.F., Hao, Q.Z., Wu, H.B., Qiao, Y.S., Zhu, R.X., Peng, S.Z., Wei, J.J., Yuan, B.Y., Liu, T.S., 2002. Onset of Asian desertification by 22 Myr ago inferred from loess deposits in China. Nature 416, 159–163.

Halbritter, H., Ulrich, S., Grímsson, F., Weber, M., Zetter, R., Hesse, M., Buchner, R., Svojtka, M., Frosch-Radivo, A., 2018. Illustrated Pollen Terminology. Second edition. Vienna, Springer.Hardenbol, J., Thierry, J., Farley, M.B., De Graciansky, P.-C., Vail, P.R., 1998. Mesozoic and Cenozoic chronostratigraphic framework of European basins. SEPM Special Publ. 60, 3–13.

Head, J.J., Gunnell, G.F., Holroyd, P.A., Hutchison, J.H., Ciochon, R.L., 2013. Giant lizards occupied herbivorous mammalian ecospace during the Paleogene greenhouse in Southeast Asia. Proc. R. Soc. B 280, 20130665.

Hel-hama, 2013. Wikipedia Commons. (https://commons.wikimedia.org/wiki/File:Burma_administrative_divisions.svg) with a CC BY-SA 3.0 license (https://creativecommons.org/licenses/by-sa/3.0/) (accessed 12 March 2021).

Herman, A.B., Spicer, R.A., Aleksandrova, G.N., Yang, J., Kodrul, T.M., Maslova, N.P., Spicer, T.E.V., Chen, G., Jin, J.H., 2017. Eocene–early Oligocene climate and vegetation change in southern China: evidence from the Maoming Basin. Palaeogeogr. Palaeoclimatol. Palaeoecol. 479, 126–137.

Hsieh, T.C., Ma, K.H., Chao, A., 2014. iNEXT: An R package for interpolation and extrapolation in measuring species diversity.

Htway, O., Matsumoto, J., 2011. Climatological onset dates of summer monsoon over Myanmar. Int. J. Climatol. 31, 382–393.

Huang, H., Licht, A., Morley, R., Dupont-Nivet, G., Zaw Win, Westerweel, J., Littell, V., Hnin Hnin Swe, Myat Kaythi, Day Wa Aung, Roperch, P., Poblete, F., Kyaing Sein, Jardine, P., Philip, A., Hoorn, C., 2018. Palynology of the central Myanmar basin corroborates Eocene–Oligocene monsoonal conditions in south-east Asia. Abstract volume of the European Palaeobotany and Palynology Conference, 12–17 August 2018, Dublin, Ireland.

Huang, H., Morley, R., Licht, A., Dupont-Nivet, G., Grímsson, F., Zetter, R., Westerweel, J., Zaw Win, Day Wa Aung, Hoorn, C., 2020. Eocene palms from central Myanmar in a South-East Asian and global perspective: evidence from the palynological record. Bot. J. Lin. Soc. 194, 177–206.

Huang, H., Pérez-Pinedo, D., Morley, R.J., Dupont-Nivet, G., Philip, A, Zaw Win, Day Wa Aung, Licht, A., Jardine, P.E., Hoorn, C., 2021. At a crossroads: The late Eocene flora of central Myanmar owes its composition to plate collision and tropical climate. Rev. Palaeobot. Palynol. 291, 104441.

International Commission on Stratigraphy (ICS), 2020. TimeScale Creator. https://timescalecreator.org/index/index.php (accessed 12 March 2021).

Jacques, F.M.B., Su, T., Spicer, R.A., Xing, Y., Huang, Y., Wang, W., Zhou, Z., 2011. Leaf physiognomy and climate: are monsoon systems different? Glob. Planet. Change 76, 56–62.

Jaramillo, C.A., Dilcher, D.L., 2000. Microfloral diversity patterns of the late Paleocene–Eocene interval in Colombia, northern South America. Geology 28, 815–818.

Jaramillo, C.A., Dilcher, D.L., 2001. Middle Paleogene palynology of central Colombia, South America: A study of pollen and spores from tropical latitudes. Palaeontogr. Abt. B 258, 87–213.

Jaramillo, C., Ochoa, D., Contreras, L., Pagani, M., Carvajal-Ortiz, H., Pratt, L.M., Krishnan, S., Cardona, A., Romero, M., Quiroz, L., Rodriguez, G., Rueda, M.J., de la Parra, F., Moron, S., Green, W., Bayona, G., Montes, C., Quintero, O., Ramirez, R., Mora, G., Schouten, S., Bermudez, H., Navarrete, R., Parra, F., Alvaran, M., Osorno, J., Crowley, J.L., Valencia, V., Vervoort, J., 2010. Effects of rapid global warming at the Paleocene–Eocene boundary on neotropical vegetation. Science 330, 957–961.

Jaramillo, C., Rueda, M.J., Mora, G., 2006. Cenozoic plant diversity in the Neotropics. Science 311, 1893–1896.

Jardine, P., 2011. Spatial and temporal diversity trends in an extra-tropical megathermal vegetation type: The Early Paleogene pollen and spore record from the U.S. Gulf Coast. Ph.D. Thesis, University of Birmingham, Birmingham, UK.

Jardine, P.E., Harrington, G.J., Sessa, J.A., Dašková, J., 2018. Drivers and constraints on floral latitudinal diversification gradients. J. Biogeogr. 45, 1408–1419.

Keating-Bitonti, C.R., Ivany, L.C., Affek, H.P., Douglas, P., Samson, S.D., 2011. Warm, not super-hot, temperatures in the early Eocene subtropics. Geology 39, 771–774.

Kershaw, A., 1997. A bioclimatic analysis of early to middle Miocene brown coal floras, Latrobe Valley, south-eastern Australia. Aust. J. Bot. 45, 373–387.

Kershaw, A.P., Nix, H.A., 1988. Quantitative palaeoclimatic estimates from pollen data using bioclimatic profiles of extant taxa. J. Biogeogr. 15, 589–602.

Klages, J.P., Salzmann, U., Bickert, T., Hillenbrand, C.D., Gohl, K., Kuhn, G., Bohaty, S.M., Titschack, J., Müller, J., Frederichs, T., Bauersachs, T., 2020. Temperate rainforests near the South Pole during peak Cretaceous warmth. Nature 580, 81–86.

Kress, W.J., DeFilipps, R.A., Farr, E., Kyi, D.Y.Y., 2003. A checklist of the trees, shrubs, herbs, and climbers of Myanmar (revised from the original works by Lace, J.H., Rodger, R. Hundley H.G., U Chit Ko Ko on the "List of trees, shrubs, herbs and principal climbers etc. recorded from Burma"). Contrib. U. S. Natl. Herb. 45, 1–590.

Lai Lai Aung, Ei Ei Zin, Pwint Theingi, Naw Elvera, Phyu Phyu Aung, Thu Thu Han, Yamin Oo, Skaland, R.G., 2017. Myanmar climate report. MET rep. 9, 1–105.

Lelono, E.B., 2000. Palynological Study of the Eocene Nanggulan Formation, Central Java, Indonesia. Ph.D. Thesis, Royal Holloway University of London, UK.

Li, S., Mao, L., Spicer, R.A., Lebreton-Anberrée, J., Su, T., Sun, M., Zhou, Z., 2015. Late Miocene vegetation dynamics under monsoonal climate in southwestern China. Palaeogeogr. Palaeoclimatol. Palaeoecol. 425, 14–40.

Licht, A., Boura, A., De Franceschi, D., Utescher, T., Chit Sein, Jaeger, J.-J., 2015. Late middle Eocene fossil wood of Myanmar: implications for the landscape and the climate of the Eocene Bengal Bay. Revi. Palaeobot. Palynol. 216, 44–54.

Licht, A., Dupont-Nivet, G., Win, Z., Swe, H.H., Kaythi, M., Roperch, P., Ugrai, T., Littell, V., Park, D., Westerweel, J., Jones, D., Poblete, F., Aung, D.W., Huang, H., Hoorn, C., Sein, K., 2019.

Paleogene evolution of the Burmese forearc basin and implications for the history of India-Asia convergence. Geol. Soc. Am. Bull. 131(5-6), 730–748.

Licht, A., France-Lanord, C., Reisberg, L., Fontaine, C., Soe, A.N., Jaeger, J.-J., 2013. A palaeo Tibet-Myanmar connection? Reconstructing the Late Eocene drainage system of central Myanmar using a multi-proxy approach. J. Geol. Soc. London, 170, 929–939.

Licht, A., van Cappelle, M., Abels, H.A., Ladant, J-B, Trabucho-Alexandre, J., France-Lanord, C., Donnadieu, Y., Vandenberghe, J., Rigaudier, T., Lécuyer, C., Terry Jr, D., Adriaens, R., Boura, A., Guo, Z., Aung Naing Soe, Quade, J., Dupont-Nivet, G., Jaeger, J.-J., 2014. Asian monsoons in a late Eocene greenhouse world. Nature 513, 501–506.

Maurin, T., Rangin, C., 2009. Structure and kinematics of the Indo-Burmese Wedge: Recent and fast growth of the outer wedge. Tectonics 28, TC2010.Metcalfe, I., 2013. Gondwana dispersion and Asian accretion: tectonic and palaeogeographic evolution of eastern Tethys. J. Asian Earth Sci. 66, 1–33.

Miller, K.G., Mountain, G.S., Wright, J.D., Browning, J.V., 2011. A 180-million-year record of sea level and ice volume variations from continental margin and deep-sea isotopic records. Oceanography 24, 40–53.

Moe Zat, Day Wa Aung, 2018. Sedimentology and Sequence Stratigraphy of Letkat Formation in Kalewa-Mawleik Area, Sagaing Region. The Second Myanmar National Conference on Earth Sciences (MNCES, 2018), 29–30 November 2018, Hinthada University, Hinthada, Myanmar.

Molnar, P., Boos, W.R., Battisti, D.S., 2010. Orographic Controls on Climate and Paleoclimate of Asia: Thermal and Mechanical Roles for the Tibetan Plateau. Annu. Rev. Earth Planet Sci. 38, 77–102.

Morley, R.J., 1996. Biostratigraphic characterisation of systems tracts in Tertiary sedimentary basins, in: Proceedings of the International Symposium on Sequence Stratigraphy in SE Asia, IPA Jakarta, pp. 49–71.

Morley, R.J., 1998. Palynological evidence for Tertiary plant dispersal in the SE Asian region in relation to plate tectonics and climate. In: Hall, R., Halloway, J.D. (Eds.), Biogeography and geological evolution of SE Asia. Backhuys, Leiden, The Netherlands, pp. 211–234.

Morley, R.J., 2000. Origin and Evolution of Tropical Rain Forests. Wiley, Chichester, UK, 362 pp.

Morley, R.J., 2012. A review of the Cenozoic palaeoclimate history of Southeast Asia. In: Gower, D.J., Johnson, K.G., Richardson, J.E., Rosen, B.R., Rüber, L., Williams, S.T. (Eds.), Biotic Evolution and Environmental Change in Southeast Asia. Cambridge University Press, Cambridge, UK, pp. 79–114.

Morley, R.J., 2013. Cenozoic ecological history of South East Asian peat mires based on the comparison of coals with present day and Late Quaternary peats. J. Limnol. 72, 36–59.

Morley, R.J., 2018. Assembly and division of the South and South-East Asian flora in relation to tectonics and climate change. J. Trop. Ecol. 34, 209–34.

Morley, R.J., 2020. Palynology in Indonesia: an overview of Quaternary studies, Cenozoic stratigraphic palynology and Sequence biostratigraphy. FOSI IAGI Webinar, 4 July 2020, online.

Morley, R.J., Bui, V.D., Nguyen, T.T., Kullman, A.J., Bird, R.T., Nguyen, V.K., Nguyen, H.C., 2019. High-resolution Palaeogene sequence stratigraphic framework for the Cuu Long Basin, offshore Vietnam, driven by climate change and tectonics, established from sequence biostratigraphy. Palaeogeogr. Palaeoclimatol. Palaeoecol. 530, 113–135.

Morley, R.J., Hasan, S.S., Morley, H.P., Jais, J.H.M., Mansor, A., Aripin, M.R., Nordin, M.H., Rohaizar, M.H., 2021. Sequence biostratigraphic framework for the Oligocene to Pliocene of Malaysia: High-frequency depositional cycles driven by polar glaciation. Palaeogeogr. Palaeoclimatol. Palaeoecol. 561, 110058.

Morley, R.J., Morley, H.P., 2010. Neogene climate history of the Makassar Straits with emphasis on the Attaka Field. Proceedings of the 34th Indonesian Petroleum Association IPA10-G-208.

Morley, R.J., Morley, H.P., Wonders, A.A.H., Sukarno, S., van Der Kaars, 2004. Biostratigraphy of modern (Holocene and Late Pleistocene) sediment cores from Makassar Straits. International Petroleum Association Proceedings, Deepwater and Frontier Exploration in Asia & Australasia Symposium, Jakarta, December 2004.

Mosbrugger, V., Utescher, T., 1997. The coexistence approach–a method for quantitative reconstructions of Tertiary terrestrial palaeoclimate data using plant fossils. Palaeogeogr. Palaeoclimatol. Palaeoecol. 134, 61–86.

Myers, N., Mittermeier, R., Mittermeier, G.C., Dafonseca, G.A.B., Kent, J., 2000. Biodiversity hotspots for conservation priorities. Nature 403, 853–858.

Nguyen, H.C., Morley, R.J., Bui, V.D., Cao, D.H.Y., Nguyen, V.S., 2011. Sequence biostratigraphy of the late Oligocene to Miocene succession in the northern Song Hong Basin, offshore Vietnam. Palaeogeogr. Palaeoclimatol. Palaeoecol. 569, 110322.

Ogg, J.G., Ogg, G., Gradstein, F.M., 2016. A Concise Geologic Time Scale. Oxford, Elsevier.

Palazzesi, L., Barreda, V., Cuitiño, J., Guler, M., Tellería, M., Santos, R.V., 2014. Fossil pollen records indicate that Patagonian desertification was not solely a consequence of Andean uplift. Nat. Commun. 5, 3558.

Pearson, P., Ditchfield, P., Singano, J., Harcourt-Brown, K.G., Nicholas, C.J., Olsson, R.K., Shackleton., N.J., Hall, M.A., 2001. Warm tropical sea surface temperatures in the Late Cretaceous and Eocene epochs. Nature 413, 481–487.

Pieters, P.E., Trail, D.S., Supriatna, S., 1987. Correlation of Early Tertiary rocks across Kalimantan, in: Proceedings Indonesian Petroleum Association 16th Annual Convention. IPA87-11/11, pp. 1–16.

Prell, W.L., Kutzbach, J.E., 1992. Sensitivity of the Indian monsoon to forcing parameters and implications for its evolution. Nature 360, 647–652.

Pross, J., Contreras, L., Bijl, P.K., Greenwood, D.R., Bohaty, S.M., Schouten, S., Bendle, J.A., Röhl, U., Tauxe, L., Raine, J.I., 2012. Integrated Ocean Drilling Program Expedition 318 Scientists. Persistent near-tropical warmth on the Antarctic continent during the early Eocene epoch. Nature 488, 73–77.

R Core Team, 2019. R: A language and environment for statistical computing. R Foundation for Statistical Computing, Vienna, Austria. https://www.r-project.org.

Ramage, C.S., 1971. Monsoon Meteorology. Academic Press, New York, United States.

Ratnam, J., Tomlinson, K.W., Rasquinha, D.N., Sankaran, M., 2016. Savannahs of Asia: antiquity, biogeography, and an uncertain future. Philos. Trans. R. Soc. Lond. B Biol. Sci. 371, 20150305.

Reichgelt, T., Kennedy, E.M., Mildenhall, D.C., Conran, J.G., Greenwood, D.R., Lee, D.E., 2013. Quantitative palaeoclimate estimates for Early Miocene southern New Zealand: evidence from Foulden Maar. Palaeogeogr. Palaeoclimatol. Palaeoecol. 378, 36–44.

Sah, S.C.D., Dutta, S.K., 1966. Palynostratigraphy of the sedimentary formations of Assam-1. Stratigraphical position of the Cherra Formation. Palaeobotanist 15, 72–86.

Saller, A.H., Noah, J.T., Ruzuar, A.P., Schneider, R., 2004. Linked lowstand delta to basinfloor Fan deposition, offshore Indonesia: An analog for deep-water reservoir systems. AAPG Bull. 88, 21–46.

Saxena, R.K., Trivedi, G.K., 2009. Palynological investigation of the Kopili Formation (Late Eocene) in North Cachar Hills, Assam, India. Acta Palaeobot. 49, 253–277.

Shaffer, B.L., 1987. The potential of calcareous nannofossils for recognizing Plio–Pleistocene climatic cycles and sequence boundaries on the shelf, in: Proceedings, Gulf Coast Section SEPM 8th Annual Research Conference, pp. 142–145.

Shukla, A., Mehrotra, R.C., Spicer, R.A., Spicer, T.E.V., Kumar, M., 2014. Cool equatorial terrestrial temperatures and the South Asian monsoon in the Early Eocene: evidence from the Gurha Mine, Rajasthan, India. Palaeogeogr. Palaeoclimat. Palaeoecol. 412, 187–198.

Smith, B., Wilson, J.B., 1996. A consumer's guide to evenness indices. Oikos 76, 70–82.

Spicer, R.A., 2017. Tibet, the Himalaya, Asian monsoons and biodiversity – In what ways are they related? Plant Divers. 39, 233–244.

Spicer, R.A., Bera, S., De Bera, S., Spicer, T.E.V., Srivastava, G., Mehrotra, R., Mehrotra, N., Yang, J., 2011. Why do foliar physiognomic climate estimates sometimes differ from those observed? Insights from taphonomic in-formation loss and a CLAMP case study from the Ganges Delta. Palaeogeogr. Palaeoclimatol. Palaeoecol. 302, 381–395.

Spicer, R.A., Herman, A.B., Liao, W., Spicer, T.E.V., Kodrul, T.M., Yang, J., Jin, J., 2014. Cool tropics in the Middle Eocene: evidence from the Changchang Flora, Hainan Island, China. Palaeogeogr. Palaeoclimatol. Palaeoecol. 412, 1–16.

Spicer, R.A., Yang, J., Herman, A.B., Kodrul, T.M., Aleksandrova, G.N., Maslova, N.P., Spicer, T.E.V., Ding, L., Xu, Q., Shukla, A., Srivastava, G., Mehrotra, R., Liu, X.Y., Jin, J.H., 2017. Paleogene

monsoons across India and South China: Drivers of biotic change. Gondwana Res. 49, 350–363.

Spicer, R.A., Yang, J., Herman, A. B., Kodrul, T., Maslova, N., Spicer, T.E.V., Aleksandrova, G., Jin, J., 2016. Asian Eocene monsoons as revealed by leaf architectural signatures. Earth Planet. Sci. Lett. 449, 61–68.

Srivastava, G., Spicer, R.A., Spicer, T.E.V., Yang, J., Kumar, M., Mehrotra, R., Mehrotra, N., 2012. Megaflora and palaeoclimate of a Late Oligocene tropical delta, Makum Coalfield, Assam: evidence for the early development of the South Asia Monsoon. Palaeogeogr. Palaeoclimatol. Palaeoecol. 342–343, 130–142.

Stamp, D.L., 1925. The Vegetation of Burma from an Ecological Standpoint. University of Rangoon, Rangoon, Myanmar.

Su, T., Spicer, R.A., Wu, F., Farnsworth, A., Huang, J., Del Rio, C., Deng, T., Ding, L., Deng, W., Huang, Y., Hughes, A., Jia, L., Jin, J., Li, S., Liang, S., Liu, J., Liu, X., Sherlock, S., Spicer, T., Srivastava, G., Tang, H., Valdes, P., Wang, T., Widdowson, M., Wu, M., Xing, Y., Xu, C., Yang, J., Zhang, C., Zhang, S., Zhang, X., Zhao, F., Zhou, Z., 2020. A Middle Eocene lowland humid subtropical “Shangri-La” ecosystem in Central Tibet. Proc. Natl. Acad. Sci. U.S.A., 117, 32989–32995.

Tang, H., Li, S., Su, T., Spicer, R.A., Zhang, S., Li, S., Liu, J., Lauretanao, V., Witkowski, C., Spicer, T.E.V., Deng, W., Wu, M., Ding, W., Zhou, Z., 2020. Early Oligocene vegetation and climate of southwestern China inferred from palynology. Palaeogeogr. Palaeoclimatol. Palaeoecol. 560, 109988.

Tardif, D., Fluteau, F., Donnadieu, Y., Le Hir, G., Ladant, J.-B., Sepulchre, P., Licht, A., Poblete, F., Dupont-Nivet, G., 2020. The origin of Asian monsoons: a modelling perspective. Clim. Past 16, 847–865.

Tardif, D., Toumoulin, A., Fluteau, F., Donnadieu, Y., Le Hir, G., Barbolini, N., Licht, A., Ladant, J.-B., Sepulchre, P., Viovy, N., Hoorn, C., Dupont-Nivet, G., 2021. Orbital variations as a major driver of climate and biome distribution during the greenhouse to icehouse transition. Sci. Adv. 7, eabh2819.

Thompson, R., Anderson, K., Pelltier, R., Strickland, L., Bartlein, P., Shafer, S., 2012. Quantitative estimation of climatic parameters from vegetation data in North America by the mutual climatic range technique. Quat. Sci. Rev. 51, 18–39.

Trenberth, K.E., Hurrell, J.W., Stepaniak, D.P., 2006. The Asian monsoon: Global perspective. In: Wang, B. (Ed.), The Asian Monsoon. Springer, New York, pp. 67–87.

van Dam, J.A., 2006. Geographic and temporal patterns in the late Neogene (12–3 Ma) aridification of Europe: the use of small mammals as paleoprecipitation proxies. Palaeogeogr. Palaeoclimatol. Palaeoecol. 238, 90–218.

van Dijk, J., Fernandez, A., Bernasconi, S.M., Rugenstein, J.K.C., Passey, S.R., White, T., 2020. Spatial pattern of super-greenhouse warmth controlled by elevated specific humidity. Nat. Geosci. 13, 739–744.

van Gorsel, J.T., Lunt, P., Morley, R.J., 2014. Introduction to Cenozoic biostratigraphy of Indonesia-SE Asia. Berita Sedimentol. 29, 6–40.

Wang, B., Ho, L., 2002. Rainy seasons of the Asian-Pacific summer monsoon. J. Clim. 15, 386–398.

Westerhold, T, Marwan, N., Drury, A.J., Liebrand, D., Angini,C., Anagnostou, E., Barnet, J.S., Bohaty, S.M., Vleeschouwer, D.D., Florindo, F., Frederichs, T., Hodell, D.A., Holbourn, A.E., Kroon, D., Lauretano, V., Littler, K., Lourens, L.J., Lyle, M., Pälike, H., Röhl, U., Tian, J., Wilkens, R.H., Wilson, P.A., Zachos, J.C., 2020. An astronomically dated record of Earth's climate and its predictability over the lasts 66 million years. Science 369, 1383–1387.

Westerweel, J., Licht, A., Cogne, N., Roperch, P., Dupont-Nivet, G., Thi, M.K., Hnin Hnin Swe, Huang, H., Zaw Win, Day Wa Aung, 2020. Burma Terrane collision and northward indentation in the Eastern Himalayas recorded in the Eocene-Miocene Chindwin Basin (Myanmar). Tectonics 39, e2020TC006413.

Westerweel, J., Roperch, P., Licht, A., Dupont-Nivet, G., Zaw Win, Poblete, F., Ruffet, G., Hin Hin Swe, Myat Kai Thi, Day Wa Aung, 2019. Burma Terrane part of the Trans-Tethyan arc during collision with India according to palaeomagnetic data. Nat. Geosci. 12, 863–868.

Willard, D.A., Donders, T.H., Reichgelt, T., Greenwood, D.R., Sangiorgi, F., Peterse, F., Nierop, K.G.J., Frieling, J., Schouten, S., Sluijs, A., 2019. Arctic vegetation, temperature, and hydrology during Early Eocene transient global warming events. Glob. Planet. Change 178, 139–152.

Xie, S., Xu, H., Saji, N.H., Wang, Y., Liu, W., 2006. Role of narrow mountains in large-scale organization of Asian monsoon convection. J. Clim. 19, 3420–3429.

Xing, Y., Utescher, T., Jacques, F.M.B., Su, T., Liu, Y.S., Huang, Y.J., Zhou, Z.K., 2012. Paleoclimatic estimation reveals a weak winter monsoon in southwestern China during the late Miocene: evidence from plant macrofossils. Palaeogeogr. Palaeoclimatol. Palaeoecol. 358–360, 19–26.

Xu, Q., Li, Y., Yang, X., Zheng, Z., 2007. Quantitative relationship between pollen and vegetation in northern China. Sci. China Earth Sci., 50, 582–599.

Yang, B., Deng, M., Zhang, M, Aung Zaw Moe, Ding, H., Mya Bhone Maw, Pyae Pyae Win, Corlett, R.T., Tan, Y., 2020. Contributions to the flora of Myanmar from 2000 to 2019. Plant Divers. 42, 292–301.

Zetter, R., 1989. Methodik und Bedeutung einer routinemäßig kombinierten lichtmikroskopischen und rasterelektronischen Untersuchung fossiler Mikrofloren. Courier Forschungsinstitut Senckenberg 109, 41–50 (in German).

Zhu, J., Poulsen, C.J., Tierney, J.E., 2019. Simulation of Eocene extreme warmth and high climate sensitivity through cloud feedbacks. Sci. Adv. 5, eaax1874.

Zizka, A., Silvestro, D., Andermann, T., Azevedo, J., Ritter, C.D., Edler, D., Farooq, H., Herdean, A., Ariza, M., Scharn, R., Svantesson, S., Wengström, N., Zizka, V., Antonelli, A., 2019. CoordinateCleaner: Standardized cleaning of occurrence records from biological collection databases. Methods Ecol. Evol. 10, 744–751.

Figure and Table Captions

Fig. 1. Maps showing the sampled sub-sections of the Yaw Formation in the Kalewa section near Kalewa Township in the Chindwin Basin (a), the position of the Kalewa section in SE Asia and Myanmar with related geographic areas and tectonic units (b), and paleogeography of the Burma Terrane at 40 Ma (c). (a) and (c) were modified after Westerweel et al. (2020), while the base map in (b) is from https://mapswire.com/. In (b) and (c), the red square shows the Kalewa section; in (b), the red circle indicates the Phiman area in Thailand for climate comparison, which the red triangle shows the Mahakam Delta, within the Kutei Basin discussed in Section 4.5. Abbreviations: BB = Bay of Bengal, BT = Burma Terrane, CB = Chindwin Basin, EAB = Eastern Andaman Basins, Fm(s). = Formation(s), GA = Gangdese Arc, GB = Greater Burma, IAT = India-Australia Transform, IBR = Indo-Burman Ranges, LT = Lhasa Terrane, MB = Minbu Basin, SB = Sibumasu, SF = Sagaing Fault, SL = Sundaland, WPA = Wuntho-Popa Arc.

Fig. 2. Maps showing modern vegetation, topography, and climate in Myanmar, with a red square showing the Kalewa area (Fig. 1). (a) Modern vegetation in India and SE Asia, from Morley (2018), which simplified from Ashton (2014). Ranges of SAM (left shaded area) and TA (right shaded area) were obtained from Spicer et al. (2017), which refers to Wang and Ho (2002). The three red circles indicate the three Asian sites (1 – the late Eocene Kopili Formation in North Cachar Hills, Assam, India; 2 – the middle to late Eocene Nanggulan Formation, central Java, Indonesia; 3 – the Zhenjiang section, Guangdong, China), plant diversity of which were compared in this study, with details in section 3.6; (b) Topography of Myanmar with the base map was modified from Helhama (2013); (c) Köppen-Geiger climate in Myanmar, after Beck et al. (2018). Abbreviations: Am = Tropical monsoon climate, Aw = Tropical savanna climate with dry-winter characteristics, Bsh = Hot semi-arid climate, Cwa = Dry-winter humid subtropical climate, Cwb = Dry-winter subtropical highland climate, Dwb = Monsoon-influenced warm-summer humid continental climate, Dwc = Monsoon-influenced subarctic climate, Et = Tundra climate (in very small mountainous regions of northern Myanmar), SAM = South Asia Monsoon, TA = Transitional area influenced by South Asia, East Asia and Western North Pacific monsoons.

Fig. 3. Magnetostratigraphy and lithologic log of the late Eocene Kalewa section, Central Myanmar Basins, and their correlation to the geomagnetic time scale. (a) Geomagnetic polarity timescale (GTS16) (Ogg et al., 2016); (b) Magnetostratigraphy indicates from Westerweel et al. (2020), and lithologic log showing lithology and the 56 pollen-productive sampling layers modified after Licht et al. (2019), with FAs 1–4 reflecting a barrier-bound, quasi-closed estuary. The Histosols are indicated as black lines in the paleosol column. Abbreviations: Vfs = very fine sand, fs = fine sand, ms = medium sand, cs = coarse sand, B = boulder. The star indicates the location of two additional

samples taken at the base of the Yaw Formation, i.e., ~250 and ~500 m below the base of the Kalewa section.

Fig. 4. Light microscopy (LM) micrographs of characteristic sporomorphs from the Kalewa section, Central Myanmar Basins. 1 and 2, *Margocolporites* spp.; 3 and 4, Sapotaceae; 5, *Meyeripollis naharkotensis*; 6, *Proxapertites operculatus*; 7, *Gothanipollis* sp.; 8, *Palmaepollenites kutchensis*; 9, *Dicolpopollis kalewensis*; 10, *Longapertites retipilatus*; 11, *Verrucatosporites usmensis*; 12, *Cupanieidites flaccidiformis*; 13, monolete spore; 14, trilete spore. 1, 3–5, 7, and 12 are from Huang et al. (2021), and 8 and 10 are from Huang et al. (2020).

Fig. 5. Scanning electron microscopy (SEM) micrographs of selected sporomorphs from the Kalewa section, Central Myanmar Basin. 1, *Proxapertites operculatus*; 2, *Spinizonocolpites prominatus*; 3, *Dicolpopollis kalewensis*; 4, *Longapertites retipilatus*; 5, *Margocolporites* sp.; 6, *Lanagiopollis emarginatus*; 7, *Discoidites* sp.; 8, *Anacolosidites reticulatus*; 9, Euphobiaceae type; 10, Sapotaceae type; 11, *Verrucatosporites usmensis*; 12, *Striatricolpites catatumbus*; 13, *Dandotiaspora* sp.; 14, *Cicatricosisporites dorogensis*. 2–4 are from Huang et al. (2020), and 5–6, 8, and 12–13 are from Huang et al. (2021).

Fig. 6. Pollen diagram with *terra firma* taxa from the late Eocene Kalewa section, Central Myanmar Basins. (a) GTS16, magnetostratigraphy, and lithology, with details referring to Fig. 3; (b) Pollen diagram with total pollen sum excluding indeterminate pollen and pollen taxa with unknown affinity, algae, and spores. The pollen sum is formed by the total count of all taxa shown here. Percentage curves are displayed with a 5 × exaggeration. Pollen zone boundaries were positioned using cluster analysis with CONISS program.

Fig. 7. Sporomorph diagram for the late Eocene Kalewa section, Central Myanmar Basin with data grouped according to vegetation type and based on the total *terra firma* sum (left) and total sporomorph sum (right) but excluding algae. (a) GTS16, magnetostratigraphy, and lithology, with details referring to Fig. 3; (b) Groups are arranged from mangrove/back-mangrove area, coastal to inland settings. Spores are displayed to the right of the *terra firma* cumulative diagram, and divided into hornworts, terrestrial wet, terrestrial dry, climbing, monolete smooth, trilete smooth, trilete ornamented, undifferentiated verrucate, and other spores. The representation of indeterminate (including poorly preserved) pollen is also shown. Percentages of *Acrostichum*, mangroves/back-mangroves and spores are presented outside the *terra firma* pollen sum and are thus shown as ratios of their counts to the pollen sum in the *terra firma* cumulative diagram. Percentages of taxa with unknown affinity and indeterminate pollen are the ratios of their counts to the pollen sum of that in the *terra firma* cumulative diagram plus themselves. Pollen zone boundaries were positioned through cluster analysis with CONISS program.

Fig. 8. Climate reconstruction with bioclimatic analysis of the late Eocene Kalewa section, Central Myanmar Basins. (a) GTS16, magnetostratigraphy, and lithology, with details referring to Fig. 3; (b) Cumulative diagram of *terra firma* taxa and pollen zones, with details referring to Fig. 7; (c) Mean annual precipitation (MAP), mean annual temperature (MAT), and monsoon intensity index (MSI) of each sample. In (c), red and black dotted lines indicate the modern-day levels of the Phiman area in Thailand, and the mean value of each pollen zone. Note that MAPs display three 'dry-wet' climatic cycles from the bottom to the top, corresponding well with the six pollen zones.

Fig. 9. Within-sample diversity (richness and evenness) of the middle to late Eocene samples from the five localities. (a) Red dots indicate the localities of the Yaw Formation (central Myanmar), the Kopili Formation (Assam, India), the Nanggulan Formation (central Java, Indonesia), the Zhenjiang section in the Maoming Basin (Guangdong, China), and the sediments in the Catatumbo and eastern Cordillera-Llanos foothill basins (Colombia); (b) Plots of expected richness (c = 0.8), Evenness (E_{var}), and Chao1 estimated richness of the five localities. Horizontal in expected richness are bootstrapped 95% confidence intervals.

Fig. 10. Schematic dip cross-section through the prograding delta of the Yaw Formation. Position of the transect (A to B) is shown in Fig. 12. The dominant swamp vegetation on the deltaic plain for each systems tract is indicated.

Fig. 11. Sequence biostratigraphic evaluation of the late Eocene Kalewa section, Central Myanmar Basins. (a) GTS16, magnetostratigraphy, and lithology, with details referring to Fig. 3; (b) Depositional sequences and corresponding systems tracts; (c) Sporomorph diagrams showing the dynamics of selected environment-indicated taxa throughout the section; (d) Geomagnetic polarity timescale (GTS16) (Ogg et al., 2016) and corresponding epoch and age; (e) Succession of late Eocene depositional sequences according to Hardenbol et al. (1998) and the coastal onlap curve of ICS (2020). Abbreviations: TST = transgressive systems tract, LST = lowstand systems tract, HST = highstand systems tract, PF = planktonic foraminifer, N = calcareous nannofossil.

Fig. 12. Catchment landscape model of the Chindwin Basin in the late Eocene Central Myanmar Basins, modified from the block diagram of Licht et al. (2019), with a yellow arrow suggesting that the IBR was still taking uplift, and a blue arrow showing the drainage system coming from northeast as in Westerweel et al. (2020). At the time the volcanoes in the Wuntho-Popa Arc were inactive and often buried (Westerweel et al., 2020). Proportions of different vegetation types are also reflected in the reconstruction. Details of the transect (A to B) are shown in Fig. 10. Abbreviations: tr. = trees, shr. = shrubs.

Table 1. Summary of pollen zones.

Table 2. Bioclimatic analysis of sporomorphs in the Yaw Formation in the Kalewa section, Central Myanmar Basins and the modern-day levels of Kalewa area and Phiman area (Thailand) estimated based on their coordinates via the WorldClim Version 2 database (https://worldclim.org/version2). Note that as Kalewa area is situated in the foothills of the Indo-Burman Ranges (IBR), it constitutes a transitional region between the central dry belt and the IBR; The estimated mean temperature of coldest quarter (MTCQ) of the modern-day level (18.9 °C) is much lower than that in the late Eocene (24.6 °C), which may be because there are mountainous areas nearby, that were incorporated in the WorldClim. Based on information from adjacent climate stations, its MAP should be 900–1700 mm, of which Kalewa climate station shows 1641 mm (Lai Lai Aung et al., 2017).

Supplementary Data Captions

Supplementary Material 1. Pollen count data (Table S1) from the late Eocene Kalewa section, Central Myanmar Basins that were used for making pollen diagrams (Figs. 6 and 7) and bioclimatic analysis (Table 2 and Supplementary Material 2), and numbers of sample/residue and England Finder positions in Figs. 4 and 5 (Table S2).

Supplementary Material 2. Pollen data (including sample information and pollen counts) (Tables S3–S7) from the five Eocene sections that were used for pollen diversity analysis and comparisons with rarefaction method.

Supplementary Material 3. Bioclimatic analysis results (Figs. S1–S10) of the late Eocene Kalewa section, Central Myanmar Basins. Full names of climatic variables are provided in Table 2.

Supplementary Material 4. Bioclimatic analysis results (Table S8) for each sample and pollen zone (mean value) from the late Eocene Kalewa section, Central Myanmar Basins. Full names of climatic variables are provided in Table 2.

Supplementary Material 5. Rarefactions results (Tables S9–S13) for the five Eocene sections shown by values in tables.

Supplementary Material 6. Rarefactions results (Figs. S11–S25) for the five Eocene sections shown by figures.

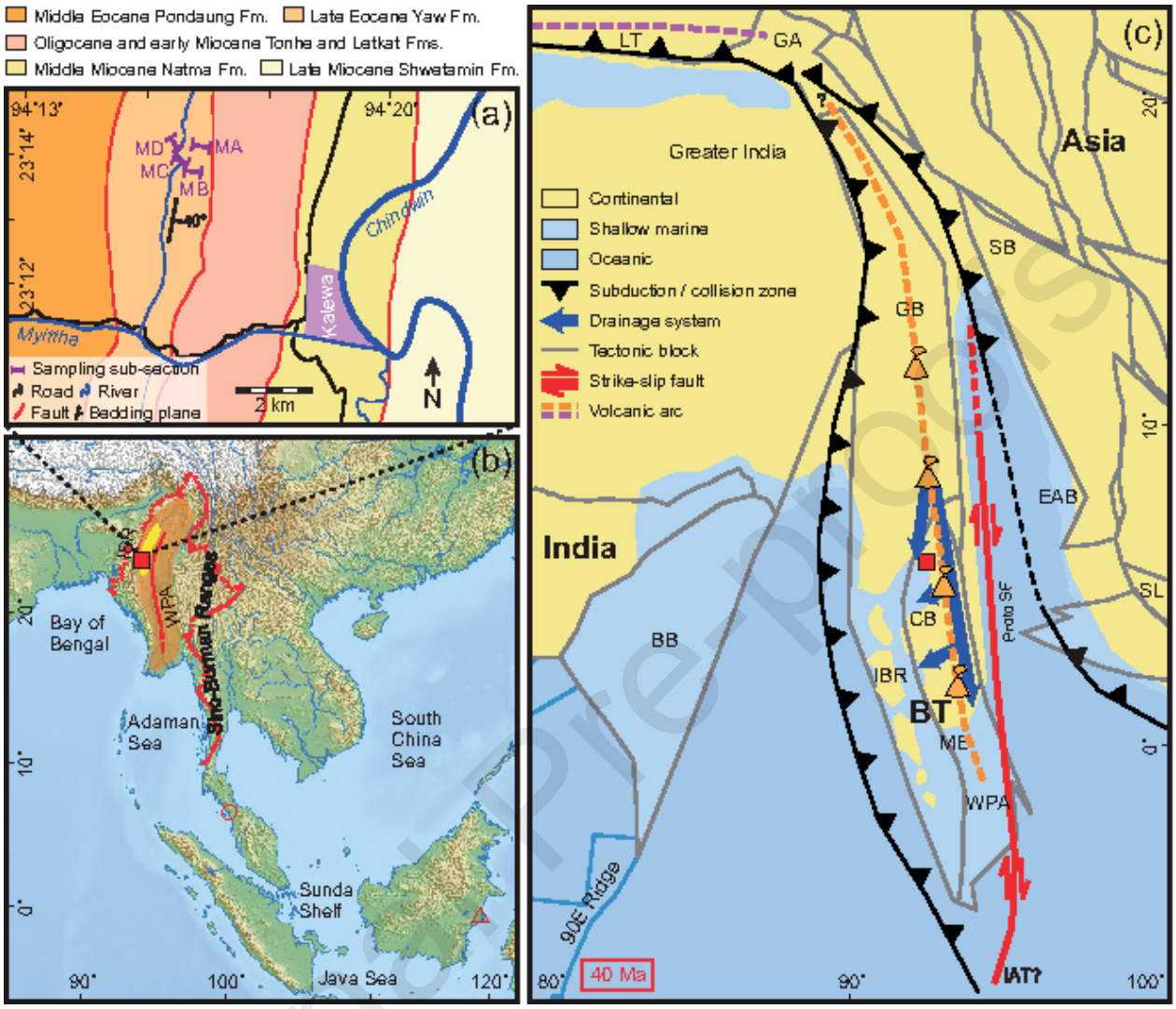

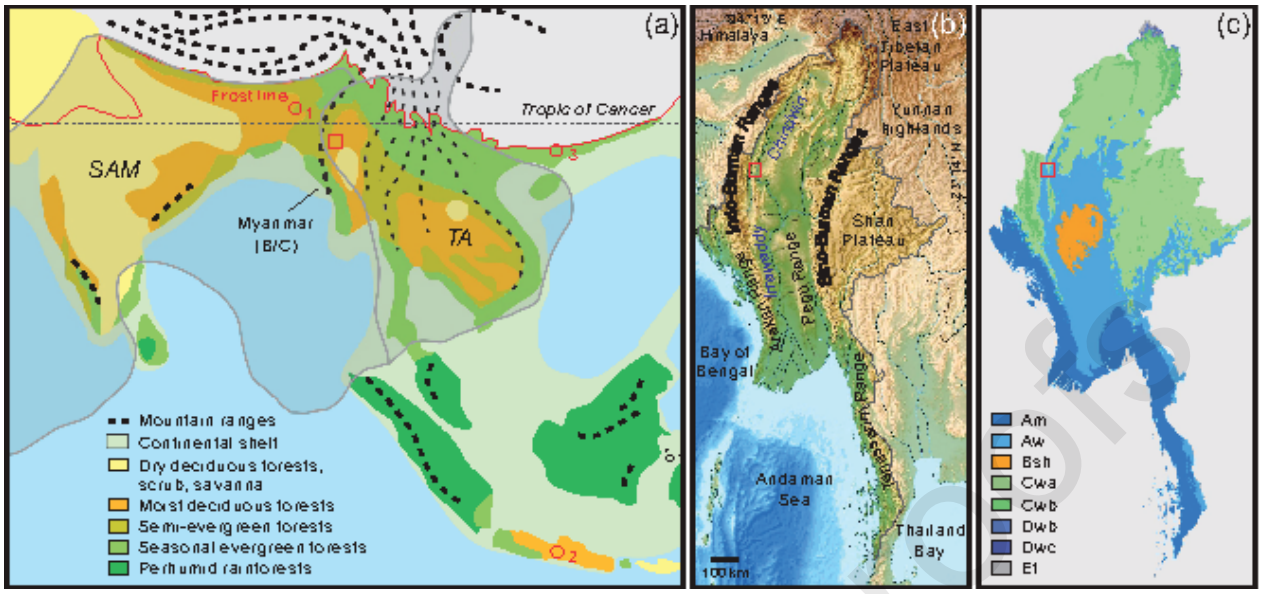

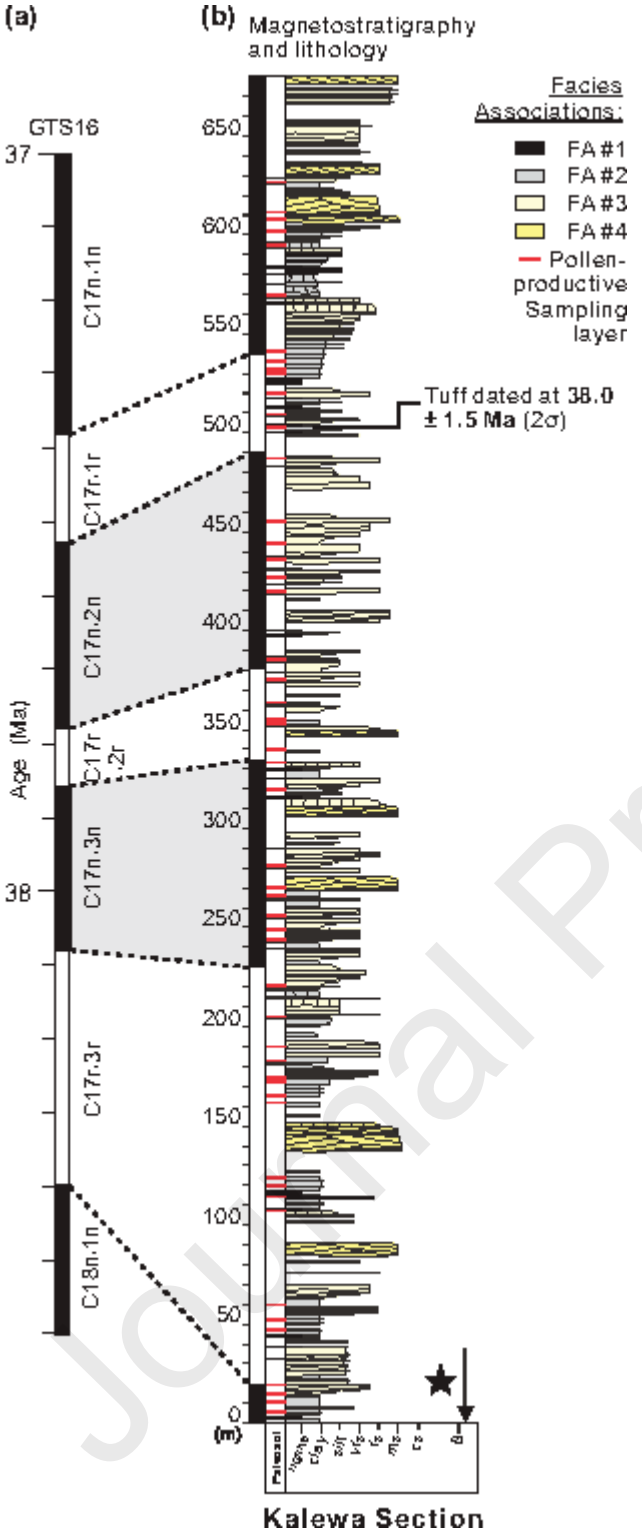

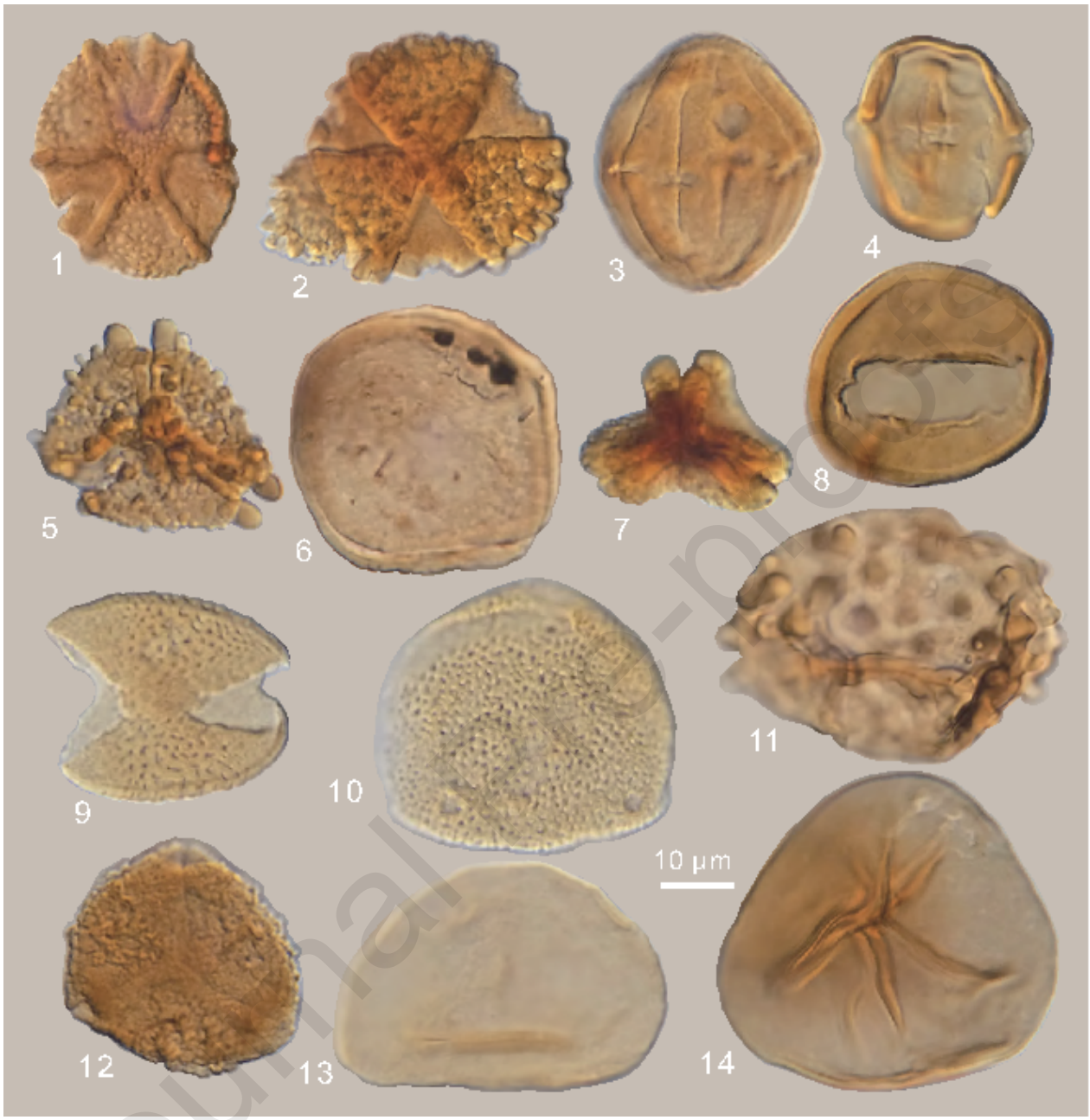

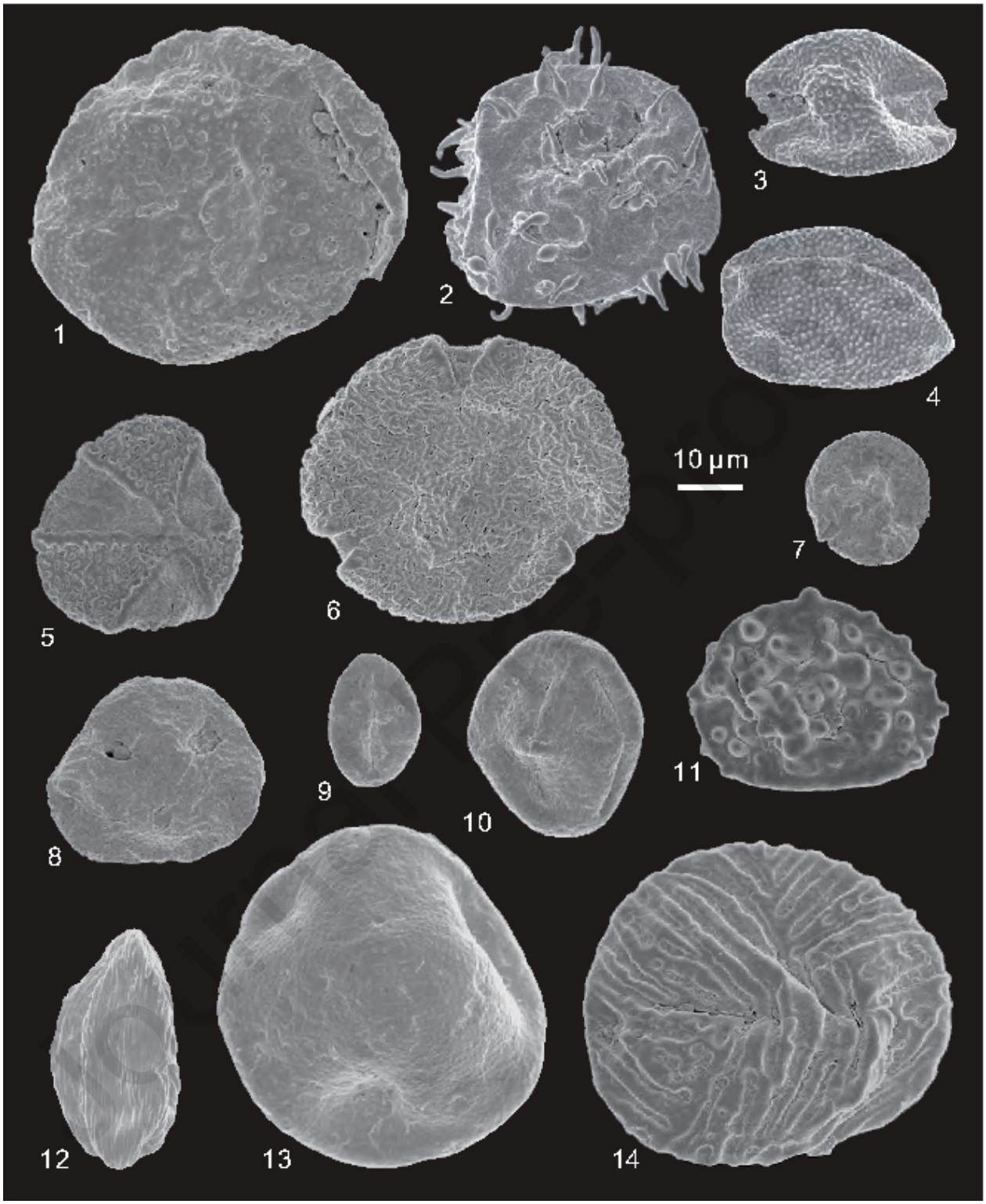
1
2
3
4
10 µm
5
6
7
8
9
10
11
12
13
14

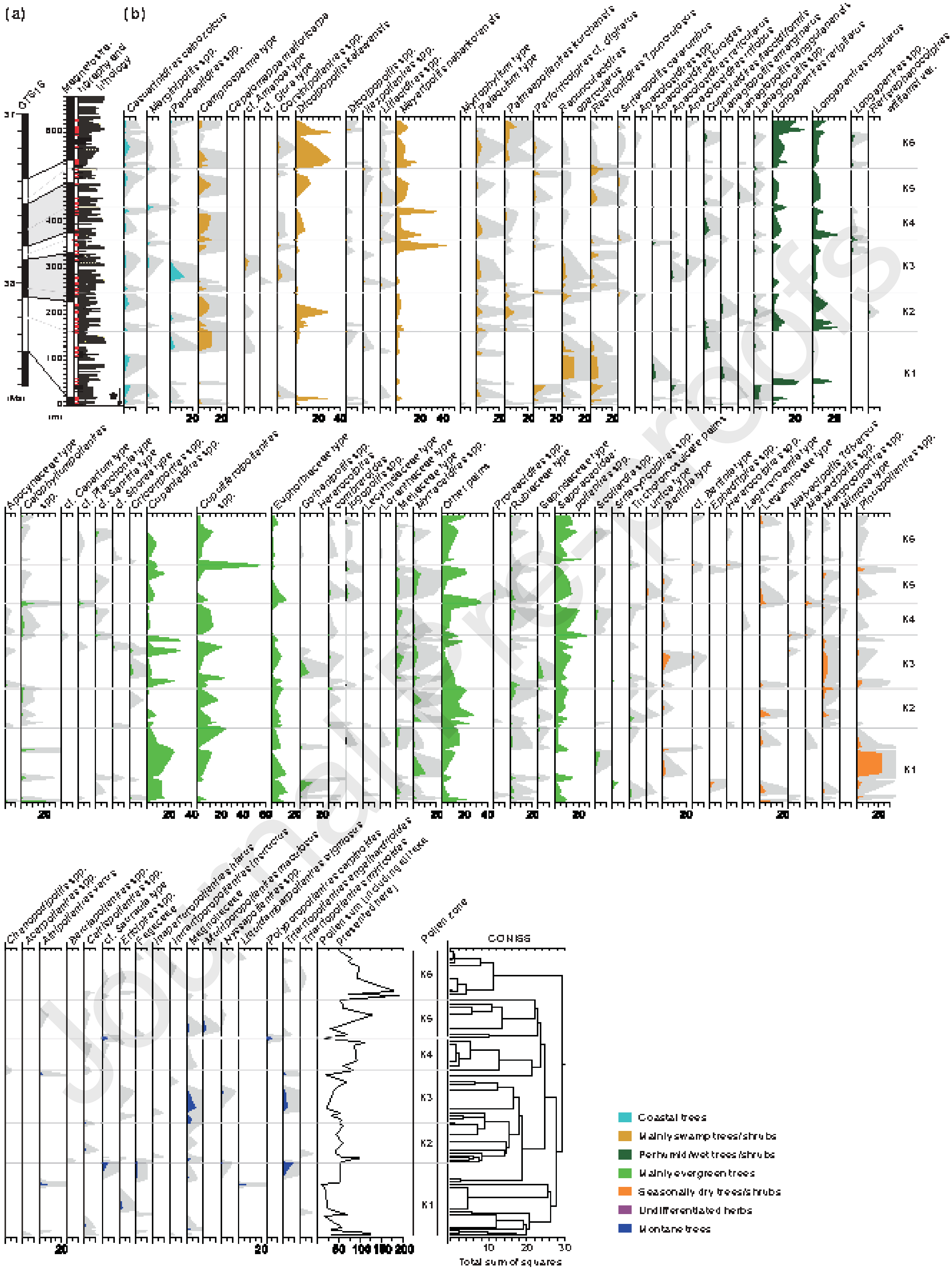

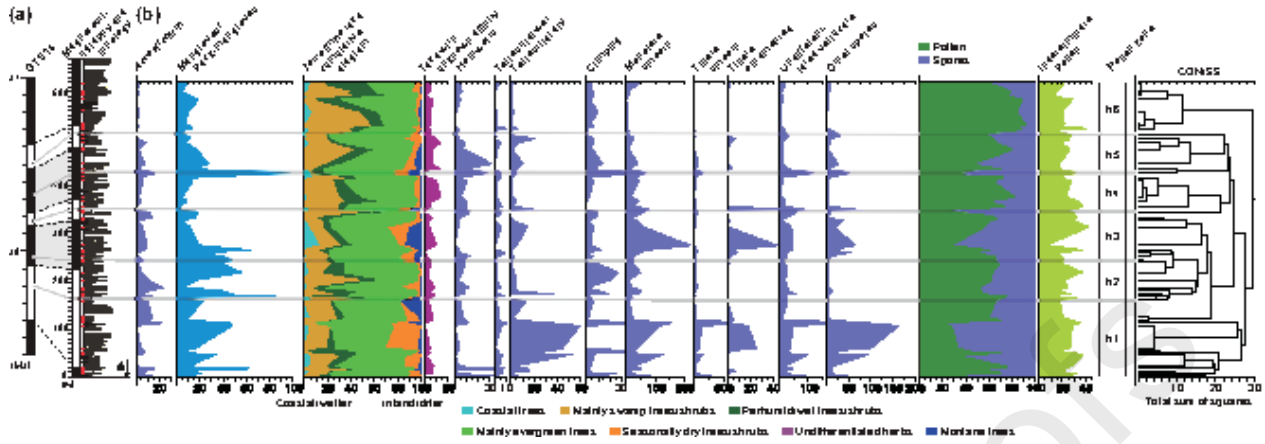

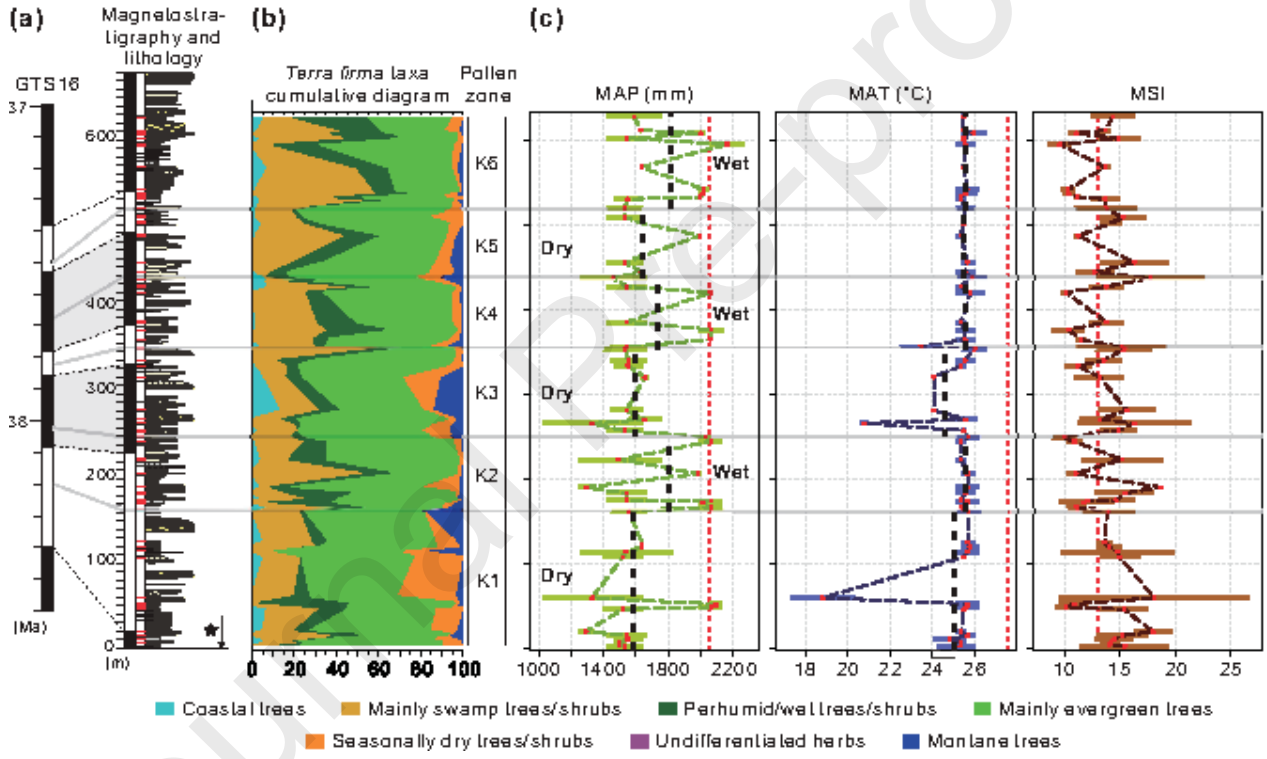

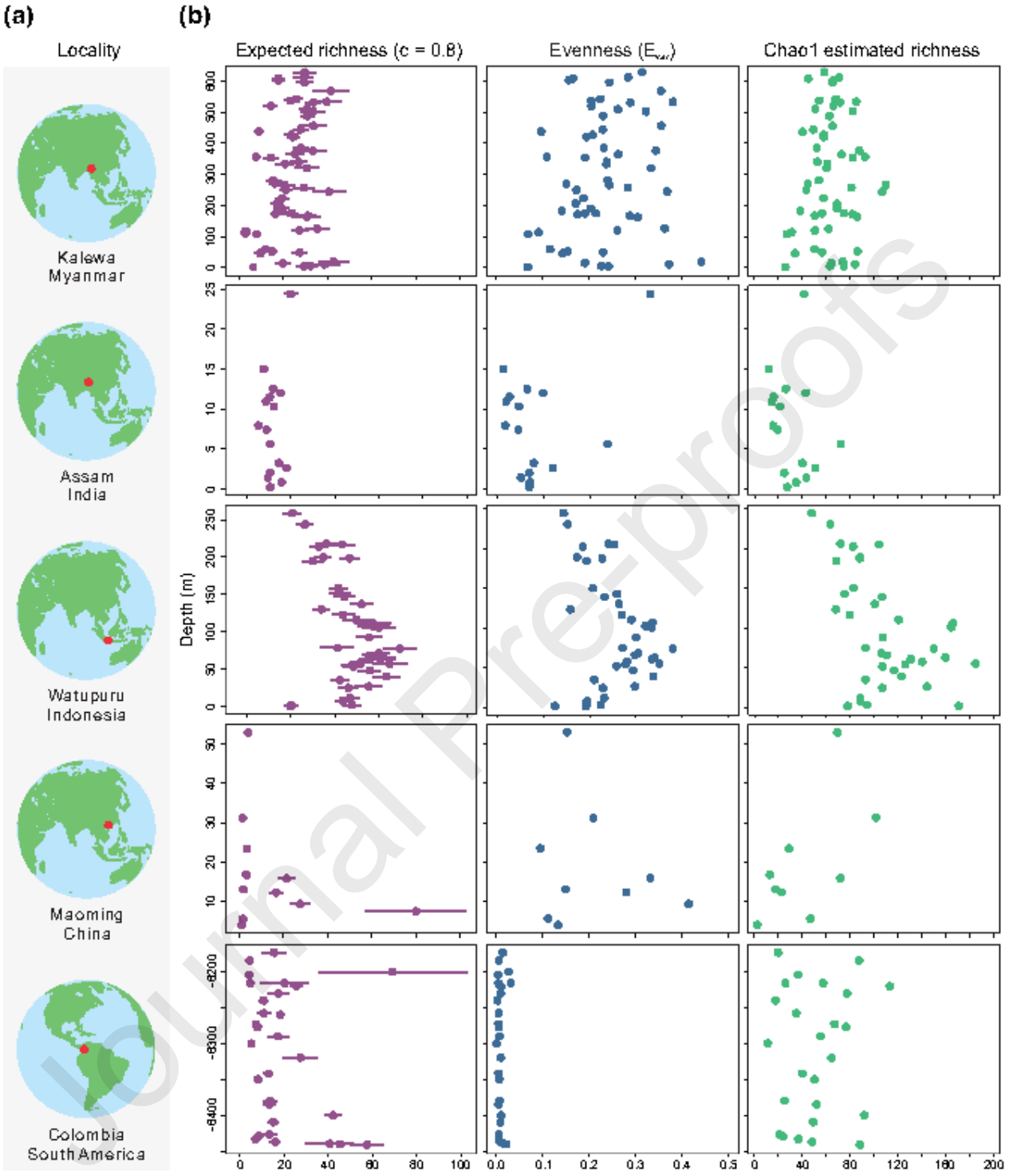

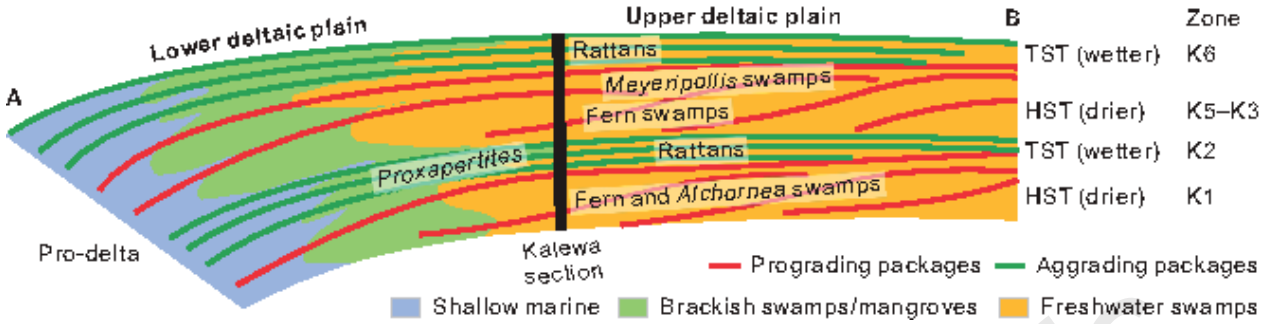

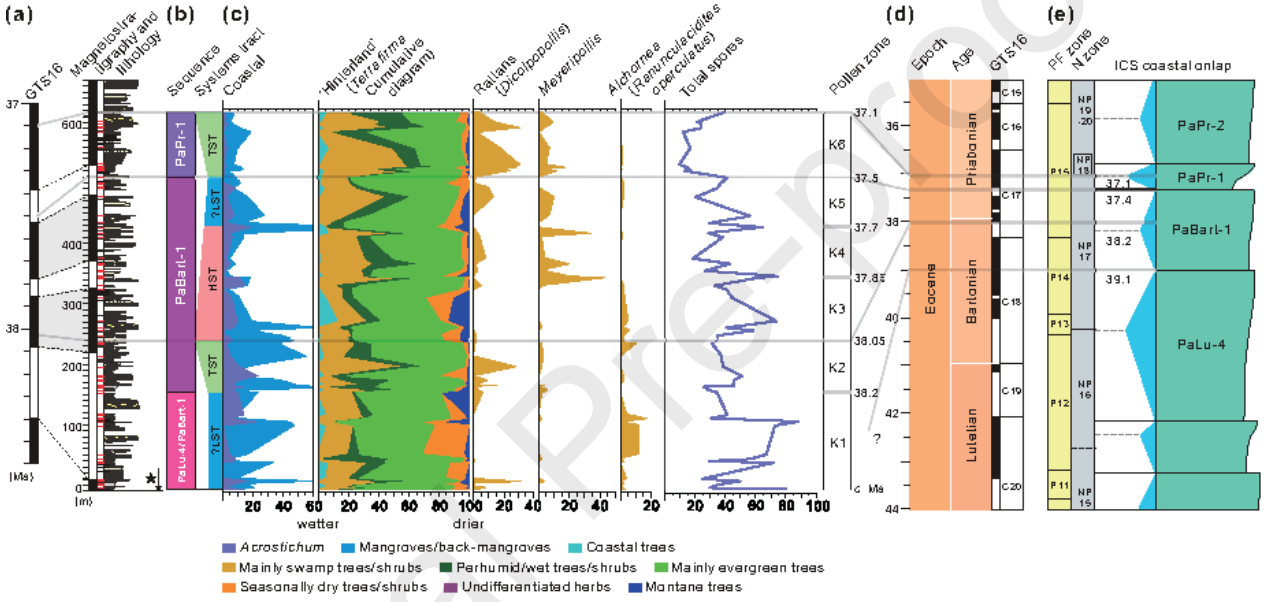

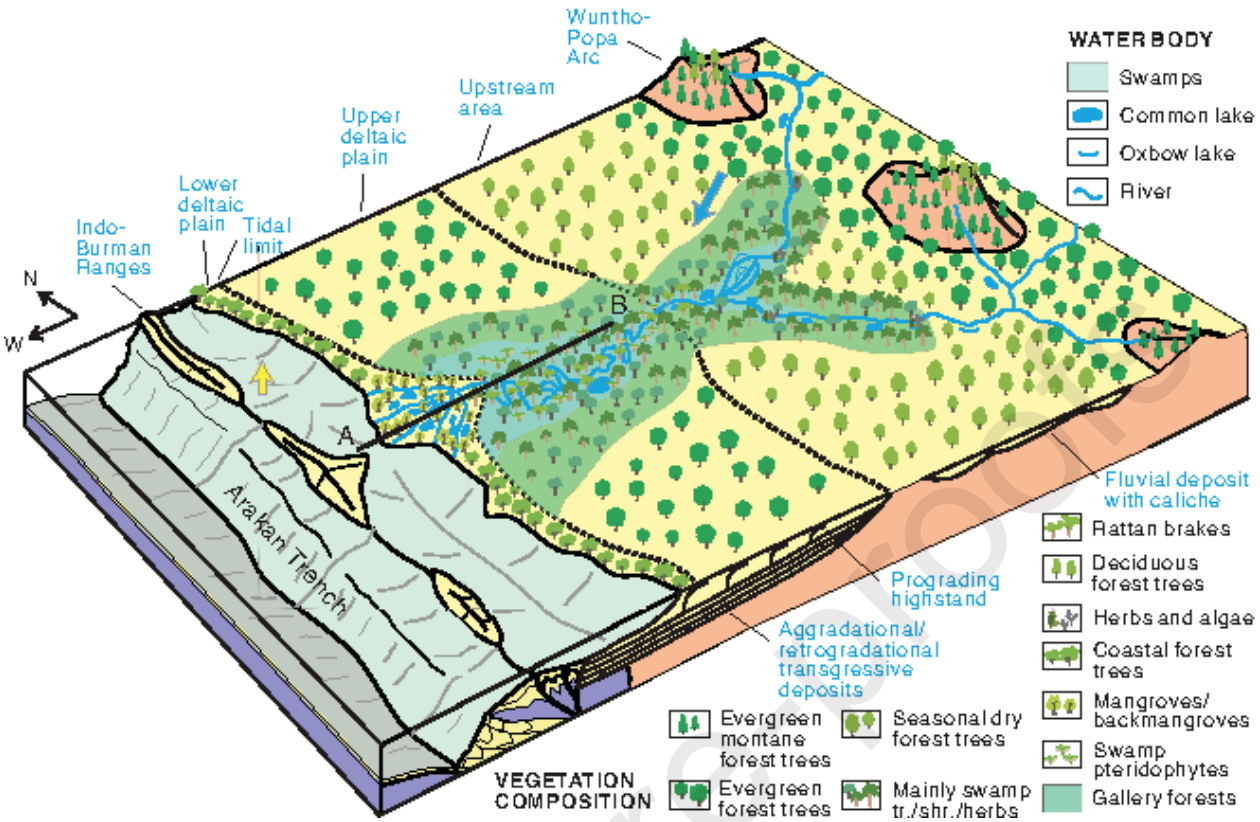

Pollen zone	Assemblage characteristics
K6 (519.2–627.5 m, *c.* 37.5 Ma)	Highest content of pollen vs. spores compared to other zones. Hinterland assemblages are dominated by *Dicolpopollis*. Mangrove/back-mangrove pollen and spores of the mangrove fern *Acrostichum* occur in low percentages.
K5 (436.7–519.2 m, *c.* 37.7–37.5 Ma)	*Meyeripollis naharkotensis* and spores of hornworts (Anthocerotales) are common.
K4 (364.6–436.7 m, *c.* 37.8–37.7 Ma)	*Meyeripollis naharkotensis* and Sapotaceae pollen are common. Pollen of swamp trees dominate.
K3 (249.4–364.6 m, *c.* 38.0–37.8 Ma)	Monolete spores are abundant. Spores of hornworts (Anthocerotales) occur in low percentages.
K2 (162.5–249.4 m, *c.* 38.2–38.0 Ma)	Mangrove pollen (*Proxapertites* and *Spinizonocolpites*) and pollen of the swamp rattan (*Dicolpopollis*) are common. Spores of the climbing fern *Stenochlaena palustris* are relatively abundant.

K1 (5.8–162.5 m, *c.* 38.2 Ma, including the two samples below the Kalewa section)	Terrestrial dry spores are common, including mostly scattered *Cicatricosisporites* spp., indicative of a well-drained environment. Seasonally dry forest elements including *Pinus* (indicated by *Pinuspollenites* spp.) and *Berlinia* type are also common. Mangroves occur in low numbers. The common occurrence of *Ranunculacidites operculatus* suggests the presence of *Alchornea* swamp.

	Climate variables	**Kalewa section (late Eocene, 5° N)**	**Kalewa area (modern-day, 23° N)**	**Phiman area, Thailand (modern-day, 6° N)**
Temperature (°C)	Mean annual temperature (MAT)	25.4–25.6	24.4	27.6
	Max temperature of warmest month (MTWM)	31.4–31.7	32.2	32.6
	Min temperature of coldest month (MTCM)	18.9–19.1	14.2	23.2
	Mean temperature of warmest quarter (MTWQ)	25.7–25.8	28.1	28.4
	Mean temperature of coldest quarter (MTCQ)	24.6	18.9	26.9
Precipitation (mm)	Mean annual precipitation (MAP)	1635–1637	1683	2053
	Precipitation of wettest month (PWETM)	282–293	338	294
	Precipitation of driest month (PDRYM)	47–54	3	33
	Precipitation of wettest quarter (PWETQ)	763–792	901	814
	Precipitation of driest quarter (PDRYQ)	209–225	18	169

Monsoon intensity index (MSI)	14–15	20	13

Declaration of interests

☒ The authors declare that they have no known competing financial interests or personal relationships that could have appeared to influence the work reported in this paper.

☐The authors declare the following financial interests/personal relationships which may be considered as potential competing interests:

Highlights

- Vegetation patterns are dominated by lowland evergreen forests and swamps.
- Global sea level change controlled environments with some successions.
- As a crossroads for India-Asia plant dispersals, Myanmar had high floristic diversity.
- A proto-monsoonal, drier and cooler climate existed with well-marked seasonality.
- Climate and tectonics shaped the vegetation, environments, and floristic diversity.